

Improved calculations of electron-ion Bremsstrahlung Gaunt factors for astrophysical applications

Jens Chluba^{1*}, Andrea Ravenni^{1†} and Boris Bolliet^{1‡}

¹*Jodrell Bank Centre for Astrophysics, School of Physics and Astronomy, The University of Manchester, Manchester M13 9PL, U.K.*

Accepted 2019 – Received 2019 –

ABSTRACT

Electron-ion Bremsstrahlung (free-free) emission and absorption occur in many astrophysical plasmas for a wide range of physical conditions. This classical problem has been studied multiple times, and many analytical and numerical approximations exist. However, accurate calculations of the transition from the non-relativistic to the relativistic regime remain sparse. Here we provide a comprehensive study of the free-free Gaunt factors for ions with low charge ($Z \leq 10$). We compute the Gaunt factor using the expressions for the differential cross section given by Elwert & Haug (EH) and compare to various limiting cases. We develop a new software package, BRpack, for direct numerical applications. This package uses a combination of pre-computed tables and analytical approximations to efficiently cover a wide range of electron and photon energies, providing a representation of the EH Gaunt factor to better than 0.03% precision for $Z \leq 2$. Our results are compared to those of previous studies highlighting the improvements achieved here. BRpack should be useful in computations of spectral distortions of the cosmic microwave background, radiative transfer problems during reionization or inside galaxy clusters, and the modeling of galactic free-free foregrounds. The developed computational methods can furthermore be extended to higher energies and ion charge.

Key words: Radiative Processes – Cosmology: cosmic microwave background – theory

1 INTRODUCTION

The Bremsstrahlung (BR) or free-free emission process is highly relevant in many astrophysical plasmas (e.g., Blumenthal & Gould 1970; Rybicki & Lightman 1979). As such it has been studied extensively in the literature (e.g., Menzel & Pekeris 1935; Karzas & Latter 1961; Brussaard & van de Hulst 1962; Johnson 1972; Kellogg et al. 1975; Hummer 1988), with early theoretical works reaching all the way back to the pioneering stages of quantum mechanics (Kramers 1923; Gaunt 1930; Sommerfeld 1931; Bethe & Heitler 1934; Sommerfeld & Maue 1935; Elwert 1939).

Bremsstrahlung is the main process responsible for the X-ray radiation of galaxy clusters (e.g., Gursky et al. 1972; Cavaliere & Fusco-Femiano 1976; Sarazin 1986); it provides a source of soft photons relevant to the thermalization of spectral distortions of the cosmic microwave background (Sunyaev & Zeldovich 1970a,b; Hu & Silk 1993; Chluba & Sunyaev 2012); and is a very important radiation mechanism close to compact objects (Shakura & Sunyaev 1973; Narayan & Yi 1995; McKinney et al. 2017). In addition it is one of the main galactic foregrounds for cosmic microwave background (CMB) temperature anisotropy studies (Planck Collaboration et al. 2016). It is thus important to have an accurate representation of this process, a problem that can be cast into computations

of the *free-free Gaunt factor*, which extend the classical Kramers formula (Kramers 1923) by quantum and relativistic corrections.

Here we are interested in typical electron energies corresponding to temperatures of $\approx 10^{-7}$ keV (a few K) up to a few tens of keV ($\lesssim 10^9$ K). This broad range of conditions is present in astrophysical plasmas of the early and late Universe (redshift $z \approx 1 - 10^9$), covering both non-relativistic and mildly relativistic thermal electron populations. Two main approaches have featured in the literature: at non-relativistic energies, the analytic expressions summarized by Karzas & Latter (1961, henceforth KL) can be applied, while at higher energies the Bethe-Heitler formula (Bethe & Heitler 1934, henceforth BH) is valid. The KL formulae provide a non-perturbative description of the BR emissivity assuming non-relativistic electron velocities¹ (i.e., electron speeds $|v|/c \ll 1$), while the BH expression utilizes the first order Born approximation ($\alpha Z \ll 1$) for relativistic electrons. Although it is well-known that higher order Coulomb corrections and shielding effects become important for high ion charge Z and extreme electron energies (e.g., Tseng & Pratt 1971; Roche et al. 1972; Haug 2008), the KL and BH formulae are accurate in their respective regimes. For intermediate energies, no simple expressions exist that allow describing the Gaunt factor in the transition between the KL and BH limits.

The computation of the KL and BH Gaunt factors and their thermal averages is fairly straightforward, and various approximations and computational schemes have been developed (Karzas &

* E-mail: jens.chluba@manchester.ac.uk

† E-mail: andrea.ravenni@manchester.ac.uk

‡ E-mail: boris.bolliet@manchester.ac.uk

¹ The ion is assumed to rest before and after the interaction

Latter 1961; Brussaard & van de Hulst 1962; Itoh et al. 1985; Hummer 1988; Nozawa et al. 1998; Itoh et al. 2002). To bridge the gap between these two limits, van Hoof et al. (2015) combined the non-relativistic KL expressions and BH formula to mimic the transition. It is, however, possible to directly model the transition using the differential BR cross section of Elwert & Haug (1969, EH hereafter). This cross section is based on Sommerfeld-Maue eigenfunction (Sommerfeld & Maue 1935) and is valid for low ion charge over a wide range of electron and photon energies. It was shown that the cross section naturally approaches the non-relativistic and relativistic limits (Elwert & Haug 1969), thus joining the two regimes. However, it still has to be integrated over the particle momenta and thermally-averaged, a task that will be studied here.

In this paper we investigate the EH expression computing the total BR Gaunt factor and thermal averages for ionic charge $Z \leq 10$, having applications to the evolution of CMB spectral distortions and the reionization process in mind, where hydrogen and helium (i.e., $Z \leq 2$) dominate. We numerically integrate the differential EH cross section and compare the obtained results to various limiting cases. The differential cross section is simplified and several new approximations are presented (Sect. 2.4). The main numerical challenge is the demanding evaluation of hypergeometric functions, which we reduce to the evaluation of one real function (see Appendix C). We in detail discuss the domains of validity of the various expressions (Sect. 3 and Sect. 4) and directly compare with previous calculations (Sect. 4.5). All our results can be reproduced with BRpack², which uses a combination of pre-computed tables and analytic approximations to efficiently represent the EH, BH and KL Gaunt factors over a wide range of electron and photon energies. A compression of the required data at low and high photon energies is achieved by analytic considerations.

2 BREMSSTRAHLUNG CROSS SECTIONS

In this section, we provide a comprehensive summary of existing analytic expressions for the BR emission cross section³. An improved expression for the differential cross section was given by EH. One crucial feature is that at high energies the EH formula naturally reduces to the BH formula, while at low energies the non-relativistic expression of KL is recovered. Thus, the EH formalism allows computing the total BR cross section for the intermediate case. However, the evaluation of the cross section is cumbersome and it is therefore crucial to understand its limiting cases.

2.1 Classical Kramers BR formula

In the classical limit, the BR cross section for the emission of a photon at energy $\omega = h\nu/m_e c^2$ by an electron with momentum p_1 reads (Kramers 1923; Karzas & Latter 1961)

$$\frac{d\sigma_K(\omega, p_1)}{d\omega} = \frac{2\alpha Z^2}{\sqrt{3}} \frac{\sigma_T}{p_1^2 \omega}. \quad (1)$$

Here, α is the fine structure constant, Z the ion charge and σ_T the Thomson cross-section. Due to energy conservation, only photons with energy $\omega \leq \omega_{\max} = \gamma_1 - 1$ can be emitted. Here $\gamma_1 = (1 + p_1^2)^{1/2}$ is the Lorentz factor of the initial electron. The ratio of the BR emission cross sections discussed in the following sections and the Kramers approximation then defines the related Gaunt factor.

² BRpack will be made available at www.chluba.de/BRpack.

³ The absorption cross section can be deduced by interchanging the roles of the initial/final electron, denoted by momenta p_1 and p_2 , respectively. All momenta and energies are expressed in units of $m_e c$ and $m_e c^2$, respectively.

2.2 Exact non-relativistic BR cross section

The exact non-relativistic (NR) BR emission cross section can be cast into the form⁴ (Karzas & Latter 1961; Hummer 1988)

$$\frac{d\sigma_{NR}(\omega, p_1)}{d\omega} = \frac{d\sigma_K(\omega, p_1)}{d\omega} g_{NR}(\omega, p_1)$$

$$g_{NR}(\omega, p_1) = \frac{\sqrt{3}}{4\pi} \mathcal{F}(\eta_1, \eta_2) G_0 \left\{ \left[\eta_1 \eta_2 + \frac{1}{2} \left(\frac{\eta_1}{\eta_2} + \frac{\eta_2}{\eta_1} \right) \right] G_0 - \frac{(1 + \eta_1^2)(1 + \eta_2^2)}{6} G_1 \right\} \quad (2a)$$

$$G_\ell(\eta_1, \eta_2, x) = (-x)^{\ell+1} (1-x)^{\frac{i(\eta_1+\eta_2)}{2}} e^{-\pi\eta_1} {}_2F_1(1+\ell+i\eta_1, 1+\ell+i\eta_2, 2\ell+2, x) \quad (2b)$$

$$\eta_i = \frac{\alpha Z \gamma_i}{p_i}, \quad x = -\frac{4\eta_1 \eta_2}{(\eta_1 - \eta_2)^2}, \quad 1-x = \frac{(\eta_1 + \eta_2)^2}{(\eta_1 - \eta_2)^2}$$

$$\mathcal{F}(\eta_1, \eta_2) = \frac{4\pi^2 \eta_1 \eta_2}{(1 - e^{-2\pi\eta_1})(1 - e^{-2\pi\eta_2})}, \quad (2c)$$

with $p_2 = \sqrt{p_1^2 + \omega(\omega - 2\gamma_1)}$. The functions G_ℓ are all real functions (see Appendix A). Since the scattered electron momentum obeys $p_2 \leq p_1$, one also has $\eta_1 \leq \eta_2$. As shown in Appendix A1, the NR Gaunt factor can be further simplified to

$$g_{NR}(\omega, p_1) \equiv -\frac{\sqrt{3}}{2\pi} \mathcal{F}(\eta_1, \eta_2) \frac{(\eta_1 + \eta_2)^2}{(\eta_1 - \eta_2)^2} G_0 G'_0 \quad (3)$$

with $G'_0 = \partial_x G_0$ evaluated at $x = -4\eta_1 \eta_2 / (\eta_1 - \eta_2)^2$. This eases the numerical computation of g_{NR} greatly because only G_0 has to be computed. In a similar manner we will reduce the EH expression to a function of G_0 and G'_0 (Appendix C).

The functions, $G_\ell(\eta_1, \eta_2)$, are rather hard to evaluate for the range of momenta we require. In particular for $\omega < 10^{-6} \omega_{\max}$ and at $p_1 < 10^{-3}$ the computations become difficult due to catastrophic cancellations of large numbers. At $p_1 > 10^{-3}$, we use simple recursion relations similar to (Karzas & Latter 1961; Hummer 1988) outlined in Appendix A3. At $\omega < 10^{-20} \omega_{\max}$ we use the soft-photon limit of Eq. (2) derived in Appendix B (where we also kept higher order terms). It can be cast into the simple form

$$g_{NR}^{\text{soft}}(\omega, p_1) \approx \frac{\sqrt{3}}{2\pi} \mathcal{F}_E(\eta_1, \eta_2) \left\{ \ln \left(\frac{4\eta_1 \eta_2}{(\eta_1 - \eta_2)^2} \right) - \text{Re}[H(i\eta_1)] \right\}$$

$$\mathcal{F}_E(\eta_1, \eta_2) = \frac{\eta_2}{\eta_1} \frac{1 - e^{-2\pi\eta_1}}{1 - e^{-2\pi\eta_2}}, \quad (4)$$

which closely matches the NR calculation even at higher frequencies (up to $\omega \approx 10^{-3} \omega_{\max}$). Here, $H(z)$ denotes the harmonic number (see Appendix B). The remaining cases can be evaluated using arbitrary number precision (e.g., with *Mathematica*). Alternatively, the differential equation for G_0 can be solved, which also directly gives G'_0 without further effort (see Appendix A2).

To quickly compute the non-relativistic Gaunt factor we tabulate it for charge $Z = 1$ as a function of p_1 and $w = \omega/\omega_{\max}$ at $p_1 \in [5 \times 10^{-8}, 10^{-3}]$ and $w \in [10^{-20}, 1]$, which in turn allows us to obtain the thermally-averaged Gaunt factor down to temperatures comparable to $T_e \approx 1$ K. Tables for the non-relativistic absorption

⁴ We modified the definitions of η_i to match the relativistic form of EH. The effects of this modification will be illustrated below and is found to slightly improve the agreement with the EH result.

⁵ This is one of the benefits of using the emission Gaunt factor as it has a finite upper limit at $\omega_{\max} = \gamma_1 - 1$.

Gaunt factor were also given by van Hoof et al. (2014) and can be reproduced using the emission Gaunt factor. The results for ionic charge $Z > 1$ can be obtained by interpolating those for $Z = 1$ using the simple mapping $g_{\text{NR}}(p_1, \omega) \rightarrow g_{\text{NR}}(p_1^*, \omega^*)$ with

$$p_i^* = \frac{p_i/Z}{\sqrt{1 + (p_i/Z)^2[Z^2 - 1]}}, \quad \omega^* = \gamma_1^* - \gamma_2^*. \quad (5)$$

Overall our procedure gives better than 0.01% numerical precision for the non-relativistic cross section at all ω and p_1 . To further improve the non-relativistic Gaunt factor one can multiply it by γ_1^2 to capture the leading order relativistic correction

$$g_{\text{NR}}^{\text{corr}}(p_1, \omega) = \gamma_1^2 g_{\text{NR}}(p_1, \omega). \quad (6)$$

As we will show this indeed improves the range of applicability of the KL formula (see Sect. 2.3 for discussion).

2.3 Bethe-Heitler cross section

At high energies ($p_1 \gtrsim 10^{-2}Z$), the Bethe-Heitler cross section (Bethe & Heitler 1934), derived using the first order Born approximation, becomes valid. It can be cast into the form⁶ (e.g., Bethe & Heitler 1934; Jauch & Rohrlich 1976)

$$\begin{aligned} \frac{d\sigma_{\text{BH}}(\omega, p_1)}{d\omega} &= \frac{d\sigma_{\text{K}}(\omega, p_1)}{d\omega} g_{\text{BH}}(\omega, p_1) \\ g_{\text{BH}}(\omega, p_1) &= \frac{\sqrt{3}}{\pi} \left[\frac{p_1 p_2}{4} - \frac{3}{8} \gamma_1 \gamma_2 \left(\frac{p_1}{p_2} + \frac{p_2}{p_1} \right) + \gamma_1 \gamma_2 L \right. \\ &\quad \left. + \frac{3}{8} \omega L \left\{ \left(1 + \frac{\gamma_1 \gamma_2}{p_1^2} \right) \frac{\lambda_1}{p_1} - \left(1 + \frac{\gamma_1 \gamma_2}{p_2^2} \right) \frac{\lambda_2}{p_2} + \omega \left[1 + \frac{\gamma_1 \gamma_2}{p_1^2 p_2^2} + \frac{\gamma_1^2 \gamma_2^2}{p_1^2 p_2^2} \right] \right\} \right. \\ &\quad \left. + \frac{3}{8} \left(\frac{\gamma_2 p_2}{p_1^2} \lambda_1 + \frac{\gamma_1 p_1}{p_2^2} \lambda_2 - 2 \lambda_1 \lambda_2 \right) \right], \quad (7) \\ \lambda_i &= \ln(\gamma_i + p_i), \quad L = \ln \left[\frac{\gamma_1 \gamma_2 + p_1 p_2 - 1}{\omega} \right]. \end{aligned}$$

Since this expression only involves elementary functions it can be evaluated very efficiently. It is equivalent to the one used in Itoh et al. (1985); Nozawa et al. (1998) and van Hoof et al. (2015) after transforming to their variables.

At low frequencies, $p_1 \simeq p_2$ and $\gamma_1 \simeq \gamma_2$, such that

$$g_{\text{BH}} \approx \frac{\sqrt{3}}{\pi} \left\{ \gamma_1^2 \left[\ln \left(\frac{2p_1^2}{\omega} \right) - \frac{1}{2} - \frac{1}{4\gamma_1^2} \right] + \frac{3}{4} \left(\frac{\gamma_1}{p_1} - \lambda_1 \right) \lambda_1 \right\}. \quad (8)$$

For increasing p_1 , this expression scales like $\simeq \gamma_1^2$, which causes a large boost of the BR emissivity. For convenience it is therefore good to absorb this extra factor into the Kramers approximation and define the BR Gaunt factor with respect to this modified Kramers approximation, i.e., $d\sigma_{\text{K}}^{\text{corr}}/d\omega = \gamma_1^2 d\sigma_{\text{K}}/d\omega$. The modified Kramers cross section can still be thermally-averaged analytically [see Eq. (19)] such that this modification does not cause any additional complications.

It is also well-known that the BH approximation can be improved by adding the so-called Elwert factor (Elwert 1939), which already appeared in Eq. (4). This then yields

$$g_{\text{BH}}^*(p_1, \omega) \approx \mathcal{F}_{\text{E}}(\eta_1, \eta_2) g_{\text{BH}}(p_1, \omega), \quad (9)$$

which improves the agreement with the EH Gaunt factor in particular in the short-wavelength limit ($\omega \simeq \omega_{\text{max}}$). In our computations we shall always use $g_{\text{BH}}^*(p_1, \omega)$ for the Bethe-Heitler limit.

2.4 Elwert-Haug cross section

Considering BR in the EH case is a lot more challenging. No analytic expression for the total cross section, $d\sigma/d\omega$, has been given. However, EH provide an expression for the differential cross section that allows us to describe the transition between the non-relativistic and relativistic regimes.

Starting from EH, but significantly rewriting the differential cross section (see Appendix C), we find

$$\frac{d^3\sigma_{\text{EH}}}{d\mu_1 d\mu_2 d\phi_2} = \frac{d\sigma_{\text{K}}(\omega, p_1)}{d\omega} \frac{d^3g_{\text{EH}}(\omega, p_1)}{d\mu_1 d\mu_2 d\phi_2} \quad (10a)$$

$$\frac{d^3g_{\text{EH}}}{d\mu_1 d\mu_2 d\phi_2} = \frac{3\sqrt{3}}{8\pi^2} p_1 p_2 \mathcal{F}(\eta_1, \eta_2) \mathcal{M}^2(\omega, p_1, \mu_1, \mu_2, \phi_2), \quad (10b)$$

where $d^3g_{\text{EH}}/d\mu_1 d\mu_2 d\phi_2$ defines the EH Gaunt factor that is differential in three angles, characterized by the direction cosines, $\mu_i = \mathbf{p}_i \cdot \mathbf{k}/p_i \omega$, and the polar angle ϕ_2 between the incoming photon and outgoing electron. After introducing the auxiliary variables:

$$\begin{aligned} \eta_{\infty} &= \alpha Z, \quad \eta_{\pm} = \eta_1 \pm \eta_2 \\ \mu_i &= \frac{\mathbf{p}_i \cdot \mathbf{k}}{p_i \omega}, \quad \mu_{12} = \frac{\mathbf{p}_1 \cdot \mathbf{p}_2}{p_1 p_2} = \mu_1 \mu_2 + \cos(\phi_2) \sqrt{1 - \mu_1^2} \sqrt{1 - \mu_2^2} \\ \pi_i &= p_i \mu_i, \quad \pi_{12} = p_1 p_2 \mu_{12}, \quad \kappa_i = 2(\gamma_i - p_i \mu_i) = 2(\gamma_i - \pi_i) \\ \chi_i &= p_i \sqrt{1 - \mu_i^2}, \quad \chi_{12} = \chi_1 \chi_2 \cos(\phi_2) \\ \tau_i &= 4\gamma_i^2 - q^2, \quad \tau_{12} = 4\gamma_1 \gamma_2 - q^2 \\ q^2 &= |\mathbf{p}_1 - \mathbf{p}_2 - \mathbf{k}|^2 = p_1^2 + p_2^2 + \omega^2 + 2[\omega(\pi_2 - \pi_1) - \pi_{12}] \\ \xi &= \left[\left(\frac{p_1 + p_2}{\omega} \right)^2 - 1 \right] \frac{q^2}{\kappa_1 \kappa_2} \equiv \frac{\tilde{\mu} q^2}{\kappa_1 \kappa_2} \\ \kappa &= \frac{\eta_+}{\eta_{\infty}} = \frac{\gamma_1}{p_1} + \frac{\gamma_2}{p_2}, \quad \rho = \frac{1}{p_1} + \frac{1}{p_2}, \end{aligned}$$

the required matrix element can be cast into the compact form

$$\begin{aligned} \mathcal{M}^2 &= \frac{1}{q^4} \left\{ \left[J_{\text{BH}} - 2 \frac{\eta_-}{\eta_+} \xi D_1 + \frac{\eta_-^2}{\eta_+^2} \xi^2 D_2 \right] \frac{\eta_+^2 G_0^2}{4(1 - \xi)^2} + J_{\text{BH}} [\xi G_0']^2 \right\} \\ J_{\text{BH}} &= \tau_1 \frac{\chi_2^2}{\kappa_2^2} + \tau_2 \frac{\chi_1^2}{\kappa_1^2} - \tau_{12} \frac{2\chi_{12}}{\kappa_1 \kappa_2} + (\chi_1^2 + \chi_2^2 - 2\chi_{12}) \frac{2\omega^2}{\kappa_1 \kappa_2} \\ D_1 &= \tau_1 \frac{\chi_2^2}{\kappa_2^2} - \tau_2 \frac{\chi_1^2}{\kappa_1^2} + (\chi_1^2 - \chi_2^2) \frac{2\omega^2}{\kappa_1 \kappa_2} + \left(\frac{L_1}{\kappa_1} + \frac{L_2}{\kappa_2} \right) \frac{\omega}{\rho} \\ D_2 &= \tau_1 \frac{\chi_2^2}{\kappa_2^2} + \tau_2 \frac{\chi_1^2}{\kappa_1^2} + \tau_{12} \frac{2\chi_{12}}{\kappa_1 \kappa_2} + (\chi_1^2 + \chi_2^2 + 2\chi_{12}) \frac{2\omega^2}{\kappa_1 \kappa_2} \\ &\quad + \frac{8\omega^2}{\kappa_1 \kappa_2} - \left(\frac{L_1}{\kappa_1} - \frac{L_2}{\kappa_2} \right) \frac{2\omega}{\rho} + L_3 \frac{\omega^2}{\rho^2} \\ L_1 &= \kappa \left[\pi_1(\pi_{12} + p_2^2) - (\pi_1 + \pi_2 - \omega) p_1 p_2 + (2 - \pi_1 \pi_2) \omega \right] \\ &\quad + 2 \frac{\omega}{p_1} (\pi_1 + \pi_2 - \omega) \\ L_2 &= \kappa \left[\pi_2(\pi_{12} + p_1^2) - (\pi_1 + \pi_2 + \omega) p_1 p_2 - (2 - \pi_1 \pi_2) \omega \right] \\ &\quad - 2 \frac{\omega}{p_2} (\pi_1 + \pi_2 + \omega) \\ L_3 &= \tilde{\mu} \omega^2 \left[1 - \frac{\pi_1 \pi_2}{p_1 p_2} + \frac{\gamma_1 + \gamma_2}{p_1 p_2} \frac{\gamma_1 + \gamma_2 + \pi_1 + \pi_2}{p_1 p_2} \right] - 2\rho^2. \quad (11) \end{aligned}$$

where G_0 and G_0' are both evaluated at $x = 1 - \xi$ in Eq. (2). Expressed in this way indeed simplifies the computation of the cross section significantly and also allows one to more directly read off limiting cases. For instance, in the BH limit, one has $\mathcal{M}^2 = J_{\text{BH}}/q^4$

⁶ Note a missing factor of 2 in the L -term of Jauch & Rohrlich (1976).

(Elwert & Haug 1969). Alternatively, the cross section in the form Appendix (C15) can be applied. Both approaches give excellent results when using the numerical method described next.

2.4.1 Numerical evaluation of the EH cross section

To evaluate the total EH cross section, we have to integrate Eq. (10a) over μ_1 , μ_2 and ϕ_2 . This is a non-trivial task even for modern computers. At low frequencies, large cancellation issues arise which can be cured using suitable variables. At both large and small values of p_1 , the evaluation of hypergeometric functions furthermore becomes cumbersome even when applying suitable transformations for the argument. Luckily, in many of the extreme cases we can resort to the non-relativistic and Bethe-Heitler formulae. Nevertheless, intermediate cases have to be explicitly computed.

Firstly, it is helpful to convert the integral over ϕ_2 into an integral over ξ . This also reduces the number of evaluations for the hypergeometric functions, which significantly improves the computational efficiency. The symmetry of the integrand in ϕ_2 implies $\int_0^{2\pi} d\phi_2 = 2 \int_0^\pi d\phi_2 = 2 \int_{\xi_{\min}}^{\xi_{\max}} \frac{d\phi_2}{d\xi} d\xi = 2 \int_0^{\Delta\xi_{\text{tot}}} \frac{d\phi_2}{d\xi} d\xi$ with

$$\Delta\xi = \xi - \xi_{\min}, \quad \cos(\phi_2) = 1 - 2 \frac{\Delta\xi}{\Delta\xi_{\text{tot}}} \quad (12a)$$

$$\Delta\xi_{\text{tot}} = \frac{4\tilde{\mu}\chi_1\chi_2}{\kappa_1\kappa_2}, \quad \frac{d\phi_2}{d\xi} = \frac{1}{\sqrt{\Delta\xi(\Delta\xi_{\text{tot}} - \Delta\xi)}} \quad (12b)$$

$$\xi_{\min} = \frac{\tilde{\mu}(p_1^2 + p_2^2 + \omega^2 + 2[\omega(\pi_2 - \pi_1) - (\pi_1\pi_2 + \chi_1\chi_2)])}{\kappa_1\kappa_2}. \quad (12c)$$

This transformation is crucial for improving the stability of the code near the maxima of $1/q^4$; however, to further improve matters one also has to use $\Delta\mu_{21} = \mu_2 - \mu_1$ instead of μ_2 . At low frequencies, the integrand picks up most of its contributions from around $\mu_1 \approx \mu_2$. Hence this variable more naturally allows us to focus evaluations around the poles. After these transformation, we also regroup contributions and analytically cancel leading order terms $\propto \mu_1$ and $\propto p_1$. As an example, for ξ_{\min} we find

$$\xi_{\min} = \frac{\tilde{\mu}}{\kappa_1\kappa_2} \left\{ \Delta p_{21}^2 - 2p_1p_2(S_1\Delta S_{21} + \mu_1\Delta\mu_{21}) + 2[p_1\Delta\mu_{21} + \Delta p_{21}(\mu_1 + \Delta\mu_{21})]\omega + \omega^2 \right\}. \quad (12d)$$

with $\Delta p_{21} = p_2 - p_1$, $S_i = \sqrt{1 - \mu_i^2}$ and $\Delta S_{21} = S_2 - S_1$. It is also important to treat the differences Δp_{21} and ΔS_{21} analytically for small ω and $\Delta\mu_{21}$.

The contributions $\propto D_i$ in Eq. (11) become small at low frequencies and do not cause any serious numerical issues. However, we have to regroup the terms in J_{BH} . We found

$$J_{\text{BH}} = 4 \left(\gamma_2 \frac{\chi_1}{\kappa_1} - \gamma_1 \frac{\chi_2}{\kappa_2} \right)^2 - \left(\frac{\chi_1}{\kappa_1} - \frac{\chi_2}{\kappa_2} \right)^2 q^2 + (\tau_{12} + 2\omega^2) \frac{\Delta\xi}{\tilde{\mu}} + (\chi_1 - \chi_2)^2 \frac{2\omega^2}{\kappa_1\kappa_2} \quad (13)$$

to provide numerically stable results. Here we used the identity $\chi_1\chi_2 - \chi_{12} = \kappa_1\kappa_2\Delta\xi/[2\tilde{\mu}]$. This procedure allows us to compute the Bethe-Heitler limit by numerical integration of the differential cross section even at extremely low frequencies ($w = \omega/[\gamma_1 - 1] \approx 10^{-14}$), highlighting the numerical precision of our method.

The computations for the EH case over a wide range of energies requires a few additional steps. The biggest remaining problem is the evaluation of terms related to the hypergeometric functions. These can be either treated by using the real functions G_0

and G'_0 like for the NR case or by expressing matters in terms of $|\mathcal{A}|^2$ and $|\mathcal{W}|^2$ (see Appendix C14 for definitions). We studied both approaches but eventually used the former in our final calculations, finding it to be more efficient as evaluation of G_0 using the differential equation approach simultaneously yield G'_0 without further effort. Both approaches gave consistent results and we also validated the various versions of writing the EH cross section given the significant steps involved in the derivation (see Appendix C).

At $w > 10^{-6}$ and also $\xi \lesssim 10^{-8}$, we used the recursion relations for G_0 and the hypergeometric function series to compute G_0 and G'_0 . At $w \leq 10^{-6}$ we tabulated G_0 and G'_0 for $\xi \in [10^{-8}, 10^7]$ every time p_1 and w changed to accelerate the evaluations. To extend the evaluation to $\xi \gtrsim 10^7$ in this regime, we used the following asymptotic expansions for G_0 and G'_0

$$G_0^2 \approx \left(\frac{1 - e^{-2\pi\eta_1}}{2\pi\eta_1} \right)^2 \left[\phi^2 + 2\eta_1^2 \frac{\phi(2 + \phi)}{\xi} \right] \\ [\xi G'_0]^2 \approx \left(\frac{1 - e^{-2\pi\eta_1}}{2\pi\eta_1} \right)^2 \left[1 - 2\eta_1^2 \frac{(1 + \phi)}{\xi} \right] \\ \phi = \ln \xi - 2 \text{Re}[H(i\eta_1)]. \quad (14)$$

Finally, instead of computing the total cross section we numerically integrate the difference with respect to the BH case (modified by the Elwert factor). This improves the numerical precision and rate of convergence. To obtain the Gaunt factors at all energies of the photon we use the standard variables (i.e., ϕ_2 and μ_2) at $w \gtrsim 10^{-2}$, which we found to perform better in this regime.

At very low photon energies ($w \lesssim 10^{-14}$), even the procedure described above was no longer sufficient. However, just like for the non-relativistic Gaunt factor, at those energies the asymptotic behavior is reached. Motivated by Eq. (4), we thus used

$$g_{\text{EH}}^{\text{soft}}(\omega, p_1) \approx \frac{\sqrt{3}}{2\pi} \mathcal{F}_E(\eta_1, \eta_2) A \left\{ \ln \left(\frac{4\eta_1\eta_2}{(\eta_1 - \eta_2)^2} \right) - B \right\}, \quad (15)$$

with the free parameters A and B to extrapolate the Gaunt factor towards low energies. In practice we use $w = 10^{-8}$ and 10^{-6} to determine the free parameters for any of the cases at $w \lesssim 10^{-10}$. Since we are able to directly compute cases down to $w \approx 10^{-14}$ we could validate these extrapolations explicitly.

Given the numerical challenges of multi-dimensional integration we expect errors to become noticeable at $\approx 10^{-4}$ relative precision. To carry out the numerical integrals we used nested Patterson quadrature rules and the CUBA library⁷. Both procedures yield consistent results. We also checked many of our results using Mathematica, however, BRPACK was found to be faster.

3 RESULTS FOR THE GAUNT FACTOR

In this section, we present our results for the BR emission Gaunt factor, illustrating its main behavior. We also determine the range of applicability of the various approximations, focusing of low-charge ions ($Z \leq 10$). In particular, the cases $Z = 1$ and 2 (hydrogen and doubly-ionized helium) are of relevance to us, as these ions are the most common in the early Universe. To present and store the results it is convenient to use $w = \omega/[\gamma_1 - 1]$ as the frequency variable, implying $w \leq 1$. Indeed, this is one of the benefits of working with the emission Gaunt factor instead of the absorption Gaunt factor, as the w is bounded from above.

⁷ <http://www.feynarts.de/cuba/>

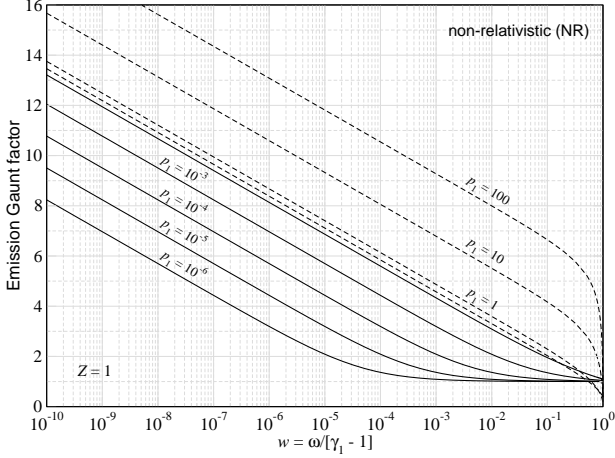


Figure 1. Non-relativistic Gaunt factor [Eq. (2)] for $Z = 1$. The usual definition relative to the Kramers formula ($d\sigma/d\omega \propto 1/[p_1^2\omega]$) is applied. The lines are for different values of p_1 , varied by factors of 10. The non-relativistic formula becomes inaccurate at $p_1 \gtrsim 10^{-1}$ (dashed lines).

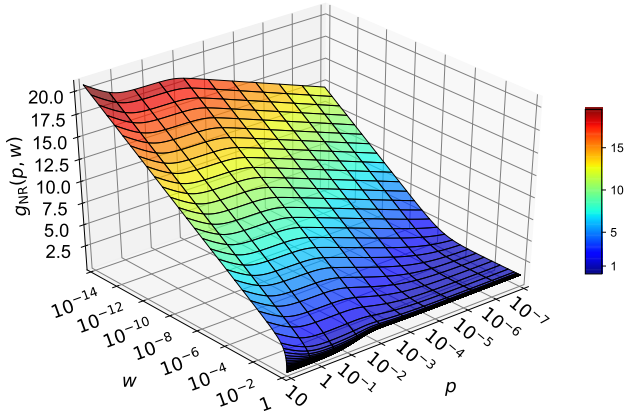


Figure 2. Numerically evaluated non-relativistic Gaunt factor [Eq. (2)] for $Z = 1$. The results for $Z > 1$ can be constructed using simple variable mapping, as given in Eq. (5).

3.1 Non-relativistic approximation

In Fig. 1, we illustrate the non-relativistic Gaunt factor for ionic charge $Z = 1$. At low photon energies, the simple asymptotic dependence given by Eq. (4) is observed. At $p_1 \approx 10^{-1}$, the non-relativistic approximation becomes inaccurate as we will see more quantitatively below (cases with dashed lines in the figure). The Gaunt factors for $Z > 1$ and $p_1 \lesssim 10^{-2}$ show similar characteristics as those for $Z = 1$. They can be obtained by simple mapping of variables [Eq. (5)], which essentially leads to $p_i \rightarrow p_i/Z$ and $\omega \rightarrow \omega/Z^2$ to leading order. For larger values of Z , additional corrections become important. A wider parameter range is covered in Fig. (2), for further illustration.

In Eq. (2) we used $\eta_i = \alpha Z \gamma_i / p_i$ instead of $\eta_i^{\text{KL}} = \alpha Z / p_i$ given in Karzas & Latter (1961). This choice is motivated by the expression of EH, which also depend this modified variable. The main difference is that at $p_1 \gtrsim 1$ (i.e., $\eta_i \rightarrow 0$) the KL expression yields a Gaunt factor that asymptotes to a constant shape. In the thermally-averaged Gaunt factor this leads to a significant drop at high photon energies as we will see below (cf., Fig. 10). This drop is not seen

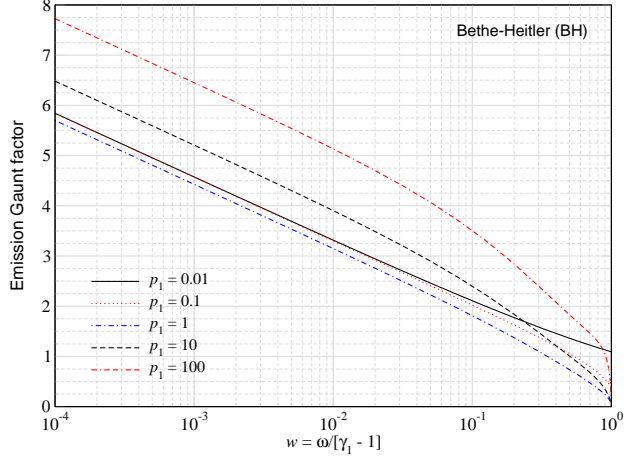


Figure 3. Relativistic Gaunt factor using the Bethe-Heitler approximation with the Elwert factor, Eq. (9). In addition to scaling the total cross section by the standard Kramers formula, we also scaled out a factor of γ_1^2 (see Sect. 2.3 for discussion). The Gaunt factor does not change significantly for electron momenta $p_1 \lesssim 10^{-2}$ and indeed is inapplicable in that regime.

for the EH result and the change of variables indeed reduces the departures. From our precomputed tables, the KL case can be obtained by simply replacing $p_i \rightarrow p_i/\gamma_i$ in the evaluation. However, in the following discussion we shall use the modified version of the NR expression, as the main conclusions do not change.

3.2 Relativistic Bethe-Heitler approximation

In Fig. 3, we illustrate the Gaunt factor in the relativistic regime using the Bethe-Heitler approximation with the Elwert factor, Eq. (9). We scaled out a factor of γ_1^2 (see discussion in Sect. 2.3) to moderate the Gaunt factor variations. As we will see below, this modification also reduces the dynamic range for the thermally-averaged Gaunt factor at high frequencies (compare Fig. 12 and 13). At low electron momenta ($p_1 \lesssim 10^{-2}$) the Bethe-Heitler formula overestimates the Gaunt factor significantly. The BH formula also does not explicitly depend on the charge Z and thus is unable to capture Coulomb corrections that become important for larger values of Z and for low values of p_1 (e.g., Elwert & Haug 1969).

3.3 Intermediate regime and domains of validity of the various approximations

For large electron momenta, the EH cross section asymptotes towards the BH formula as long as Z is not too large (i.e., $Z \lesssim 10$). To illustrate the Gaunt factor based on the expressions given by EH, it is thus convenient to compare the values directly to the BH formula. In Fig. 4, we present the results for various electron momenta $p_1 = \{0.01, 0.012, 0.015, 0.02, 0.03, 0.04, 0.05, 0.1, 0.3\}$. Note that some of the curves are not labeled explicitly and that for the NR case only those for $p_1 \leq 0.05$ are presented as the others significantly underestimate the EH result.

For $Z = 1$, the departures of the EH Gaunt factor from the BH approximation are smaller than 8% for the chosen p_1 values. Even the NR formula works very well up to⁸ $p_1 \approx 0.05$. As expected,

⁸ This conclusion is not changed significantly when using the original version for the non-relativistic Gaunt factor with $\eta_i = \alpha Z / p_i$.

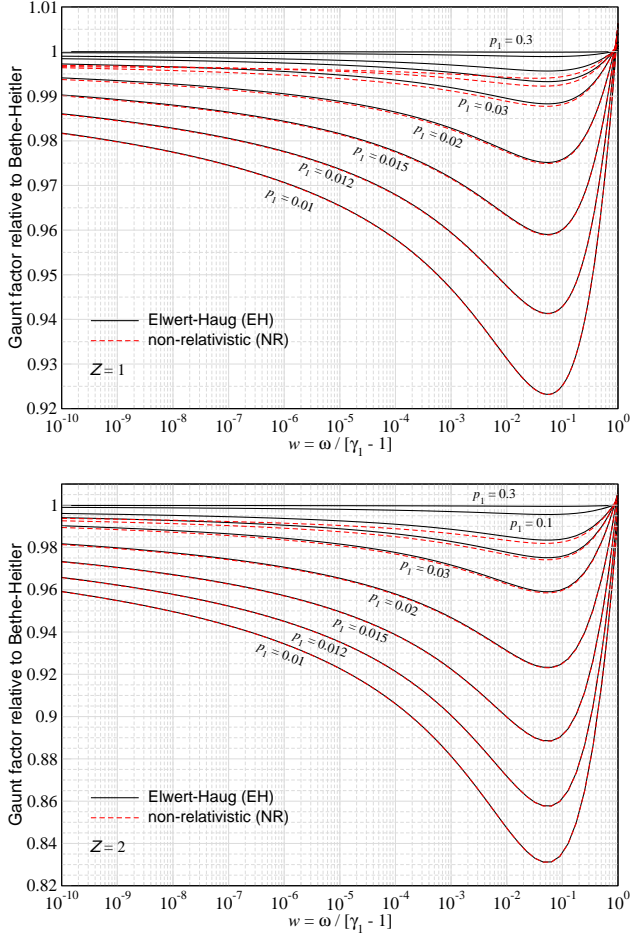


Figure 4. Comparison of the Elwert-Haug and non-relativistic Gaunt factors with the Bethe-Heitler formula for $Z = 1$ (upper panel) and 2 (lower panel). At $p_1 \approx 0.01$ the NR and EH Gaunt factors agree extremely well while for $p_1 \gtrsim 0.03$ the NR Gaunt factor underestimates the EH result. The EH formula converges towards the BH approximation at $p_1 \gtrsim 0.2 - 0.3$.

the EH formula approaches the BH cross section at $p_1 \gtrsim 0.2 - 0.3$, corresponding to kinetic energies in excess of $E_1 \approx 10$ keV. For charge $Z = 2$ (lower panel of Fig. 4), similar trends can be observed, however, the departures from the BH formula generally are bigger for fixed p_1 since $p_1^* \approx p_1/Z$ reduces. This means that for larger values of Z , the Gaunt factor remains closer to the NR case up to larger values of p_1 , i.e., $g_{\text{EH}}(p_1, \omega, Z) \approx g_{\text{EH}}(p_1/Z, \omega/Z^2, Z = 1)$.

To more quantitatively assess the validity of various approximations we ran comparisons for the Gaunt factors asking when they depart by more than a fixed relative precision from the EH calculation. The results of this comparison for $Z = 1$ are summarized in Fig. 5. As expected, the Bethe-Heitler formula correctly approximates the cross section in the relativistic regime (blue region), namely above $p_1 \gtrsim 0.05 - 0.15$ if we require a maximum 1‰ deviation (middle panel). Relaxing this requirement (bottom panel), the region in which BH is valid overlaps with the region, in red, where the non-relativistic (NR) approximation is applicable, i.e., the two approximations depart from each other by less than 2%. For clarity we mention that in the purple areas mark the overlap of the red (NR) and blue (BH) regions. Our improved NR approximation, i.e., Eq. (6), which takes into account the leading order relativistic correction, significantly enlarges the applicability of the

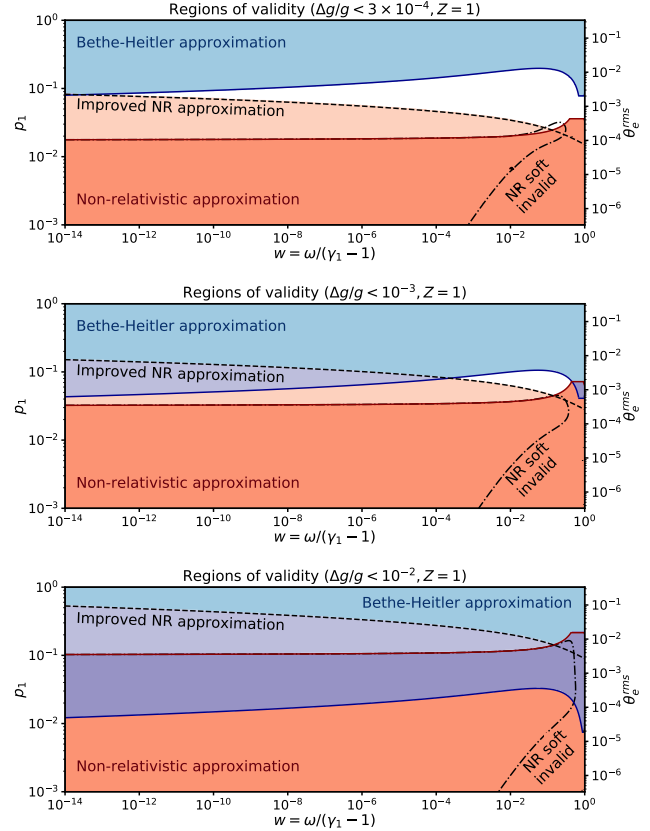


Figure 5. Regions in which the NR approximations and BH formula are valid. The colored areas are the (p_1, w) sub-spaces where the relative difference between the EH Gaunt factor and the labeled formula is less than 0.3‰ (Top panel), 1‰ (Middle panel), or 1% (Bottom panel). The white area is where the calculation using the EH Gaunt factor is required to achieve the required precision. The improved NR approximation significantly extends the reach of the NR expression. The root-mean-square temperature $\theta_e^{\text{rms}} = kT_e^{\text{rms}}/m_e c^2 = p_1^2/3$ is shown for comparison.

NR formula (orange area). We also highlight that the NR soft photon approximation, Eq. (4), works extremely well below and to the left of the dot dashed line; for higher photon energies the respective full expression has to be evaluated.

The presence of regimes in which neither the NR limit nor the BH approximations are valid (white areas in Fig. 5) makes it clear that any precise calculation involving bremsstrahlung processes needs to carefully assess when the simplified expressions can be used, and eventually resort to the EH cross section evaluation in the intermediate regime. It is however impressive that for $Z = 1$ at 1‰ precision only the BH and NR expressions are needed and a simple switch at $p_1 \approx 0.05$ should suffice when combining these two. With BRpack all cases can be efficiently modeled using one function evaluation with appropriate arguments.

For $Z = 2$, we reach similar conclusions as for $Z = 1$ (Fig. 6). The regions requiring the full EH evaluation slightly increase given the importance of terms $\propto \alpha Z$. Overall, the boundary of the NR approximation shifts roughly by a factor of 2, which is expected from $g_{\text{EH}}(p_1, \omega, Z) \approx g_{\text{EH}}(p_1/Z, \omega/Z^2, Z = 1)$. Again at 1‰ precision the BH and NR formulae are sufficient for representing the intermediate Gaunt factor, while at $\lesssim 0.1\%$ the EH result is needed. With BRpack all cases can be considered and compared.

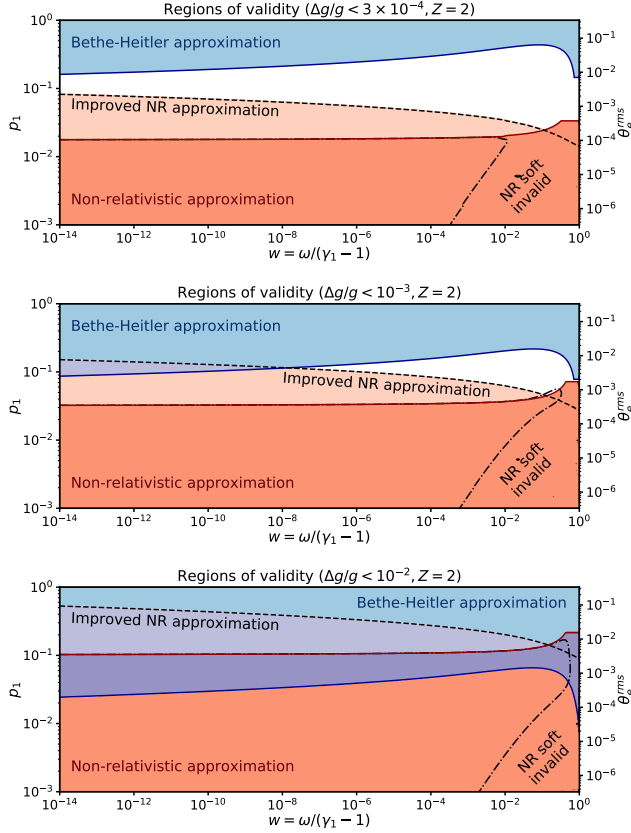


Figure 6. Same as in Fig. 5 but for $Z = 2$. The areas requiring the full EH evaluation slightly increased. Also, in comparison to $Z = 1$, the boundary of the NR formula is shifted downward by roughly a factor of 2.

3.4 Gaunt factors for $2 < Z \leq 10$

We have seen that for $Z = 1$ and 2, the departures from the EH calculation only become visible at the $\lesssim 0.1\%$ level (Fig. 5 and 6). For larger ion charge, corrections become increasingly important ultimately exceeding the 1% level. Here we restrict our discussion to cases with $Z \leq 10$ as higher order Coulomb corrections are expected to become relevant for larger ion charge (Roche et al. 1972; Haug 2008, 2010), a problem that we leave to future work.

In Fig. 7, we show the domains in which the full EH Gaunt factor evaluation is required to achieve 1% precision. For $Z = 3$ we find that a combination of the BH and NR Gaunt factors remains sufficient at this precision, but for $Z = 4$ a small domain requiring the EH evaluation appears. As expected, this domain grows with increasing charge Z . For $Z = 10$, one expects $\approx 1\%$ corrections over a significant range of photon energies at $p_1 \approx 0.2$, corresponding to rms temperature $T_e \approx 10^8$ K ($\theta_e \approx 0.02$).

When tightening the precision requirement to 0.1%, we obtain the domains shown in Fig. 8. We only computed the EH Gaunt factor up to $p_1 = 2$ (kinetic energy ≈ 600 keV), finding that for $Z \geq 7$ and $10^{-3} \lesssim w \leq 1$ the BH formula is inaccurate. Since for higher kinetic energies, additional corrections become important (e.g., Haug 2010), we limited our tables to $p_1 \leq 2$. For accurate and efficient representation of the EH Gaunt factor, BRPACK can be used at $\approx 0.01\%$ numerical accuracy up to $p_1 = 2$. Above this value of p_1 , we resort to the BH formula. This causes inaccuracies in the high frequency tail of the thermally-averaged Gaunt factor, as we explain below. However, the differences are limited to $\lesssim 0.1\%$ for $Z \leq 4$, and remain smaller than 0.5% even for $Z \leq 10$ (see Fig. 9).

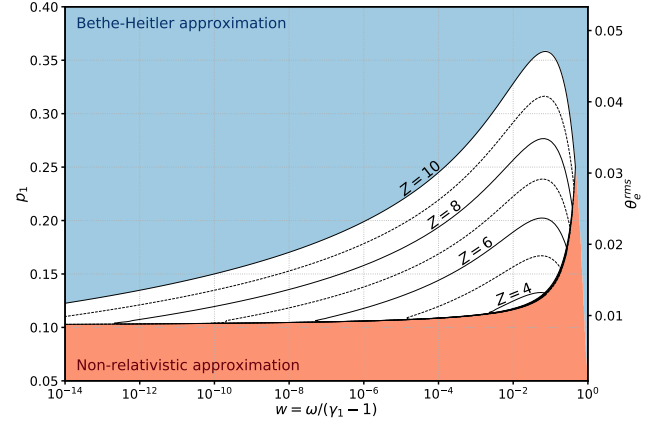


Figure 7. Regions requiring EH evaluation to achieve 1% accuracy for ion charges $Z = 4 - 10$. BRPACK allows representing the Gaunt factor over the whole domain. The colored regions, where approximations can be safely used, refer to the case for $Z = 10$.

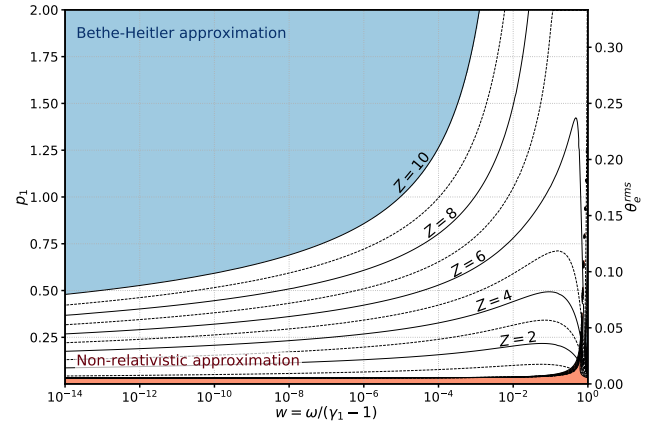


Figure 8. Same as Fig. 7 but for precision 0.1%. At this precision, the BH formula is inaccurate for $Z \geq 7$ and $10^{-3} \lesssim w \leq 1$. The non-relativistic region is quite narrow (orange region) for the considered temperatures.

3.5 High electron momenta

In our discussion, we only considered cases up to electron momenta $p_1 = 2$. For $Z = 10$, this already revealed that the BH formula is inaccurate at the level $\approx 0.1\%$ in the short-wavelength limit. Using the EH cross section, we can explore this aspect a little further. In Fig. 9, we illustrate the departures of the EH Gaunt factor from the BH formula for $w = 10^{-2}$ and $w = 1$ and several values of Z . For $Z = 4$, this shows that even up to very high electron momentum, the EH Gaunt factor does not depart by more than 0.1% from the BH formula. This statement extends to the cases $Z < 4$. BRPACK, which only contains tables up to $p_1 = 2$, thus represents the EH Gaunt factor to better than $\lesssim 0.1\%$ for $Z \leq 4$. For $Z \leq 2$, even a precision $\lesssim 0.03\%$ can be guaranteed.

At $Z > 4$, the departures of the EH Gaunt factor from the BH formula exceed the level of 0.1% in the short-wavelength limit ($\omega \approx \gamma_1 - 1$). For $Z > 4$ and $w \approx 1$, BRPACK thus does not reproduce the EH Gaunt factor at $p_1 > 2$ beyond the $\approx 0.5\%$ level. This causes inaccuracies in the thermally-average EH Gaunt factor at very high photon energies (see next Section). At lower values of w , the BH limit is again approached, with departures $\lesssim 0.15\%$ at $p_1 > 2$,

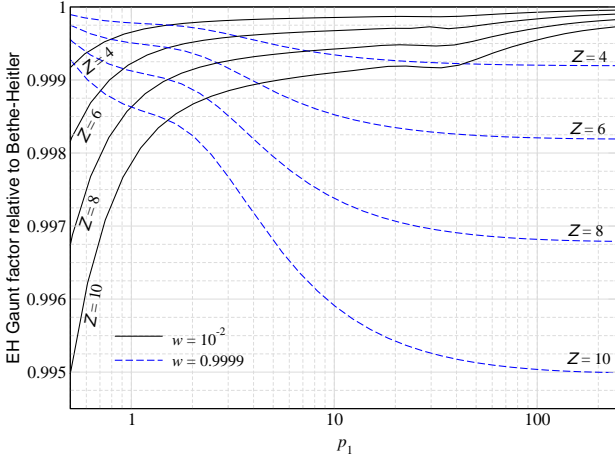


Figure 9. EH Gaunt factor relative to BH formula for $w = 10^{-2}$ and $w = 1$ as a function of p_1 and varying values of Z . At low photon energies, the EH expression clearly approached the BH formula when increasing p_1 , while in the short-wavelength limit departures from the BH formula remain visible in the shown range of p_1 .

$w \leq 10^{-2}$ and $Z \leq 10$. Therefore the low frequency tail of the EH Gaunt factor should be reproduced to high precision.

We emphasize again that with BRPACK we did not attempt to represent the EH Gaunt factor at $p_1 > 2$ more rigorously as it is clear that other corrections will also become relevant there. However, at those energies, the total number of emitted photon is exponentially small, such that this should not cause any major limitations for most applications.

4 THERMALLY-AVERAGED GAUNT FACTORS

Describing the interactions of photons and electrons in the general case is quite complicated. However, for many astrophysical applications, one can neglect anisotropies in the medium (at least locally) and simply describe the evolution of the average electron and photon distribution functions. Coulomb interactions further drive the electron distribution quickly towards a relativistic Maxwell-Boltzmann distribution function [see Eq. (18) below]. Electron-ion degeneracy effects can furthermore be neglected (but can be easily added) unless temperatures in excess of the pair-production threshold are being considered. In particular for the evolution of CMB spectral distortions, the above conditions are the most relevant (e.g., Chluba & Sunyaev 2012; Chluba 2014; Lucca et al. 2019).

4.1 Average BR emissivity in the Kramers limit

To define the thermally-averaged Gaunt factors we first introduce the averaged BR photon production term of the plasma:

$$\frac{dN_\gamma}{dt d\omega} \Big|_{\text{em}} = N_i N_e \int p_1^2 f(p_1) |v_{\text{rel}}| \frac{d\sigma(\omega, p_1)}{d\omega} dp_1. \quad (16)$$

Here, N_i the ion number density of charge Z ; N_e the electron number density corresponding to the electron momentum distribution function, $f(p_1)$, which we normalized as $\int p_1^2 f(p_1) dp_1 = 1$. The relative speed of the colliding particles is further given by $|v_{\text{rel}}| = cp_1/\gamma_1$, which becomes $|v_{\text{rel}}| \approx cp_1$ in the non-relativistic limit. Equation (16) assumed that the ions are at rest (i.e., recoil effects due to the finite mass of the nucleus can be neglected) and

that the momentum distribution of the electrons is described in this frame. Inserting the Kramers cross section, Eq. (2), into Eq. (16) the BR emissivity in the classical limit then reads

$$\begin{aligned} \frac{dN_\gamma}{dt d\omega} \Big|_{\text{em}}^{\text{K}} &\approx \frac{2\alpha Z^2}{\sqrt{3}} \frac{N_e N_i \sigma_{\text{TC}}}{\omega} \int_{p_{\text{min}}}^{\infty} p_1 f(p_1) dp_1 \\ &\approx \frac{2\sqrt{2}\alpha Z^2}{\sqrt{3}\pi\theta_e} \frac{N_e N_i \sigma_{\text{TC}}}{\omega} e^{-\omega/\theta_e}, \end{aligned} \quad (17)$$

where p_{min} is the minimal electron momentum that is required to produce a photon of energy $\omega = \hbar\nu/m_e c^2$. This is determined by $\omega = \gamma_{\text{min}} - 1$, which yields $p_{\text{min}} = \sqrt{\omega(2+\omega)} \approx \sqrt{2\omega}$. In the last step of Eq. (17) we used a non-relativistic Maxwell-Boltzmann distribution function, $f_{\text{nr}}(p) = \sqrt{2/\pi} \theta_e^{-3/2} e^{-p^2/2\theta_e}$ with dimensionless electron temperature $\theta_e = kT_e/m_e c^2$ to carry out the integral.

The expressions above explicitly assume $p_1, \omega \ll 1$. Even without quantum corrections, to generalize the Kramers approximation to higher temperatures / energies, we shall use the relativistic Maxwell-Boltzmann distribution function

$$f_{\text{rMB}}(p) = \frac{e^{-\gamma(p)/\theta_e}}{K_2(1/\theta_e)}, \quad (18)$$

where $K_2(x)$ is the modified Bessel function of second kind⁹. We also keep the full relativistic expression for $|v_{\text{rel}}| = cp_1/\gamma_1$ and furthermore realize that at low frequencies the overall BR cross section scales as $\approx \gamma_1^2/[p_1^2\omega]$ towards higher electron energies (see discussion about Bethe-Heitler limit). Thus, after multiplying the Kramers approximation, Eq. (2), by γ_1^2 and carrying out the thermal average with the above modification, we have the relativistically-improved Kramers approximation for the BR emissivity:

$$\frac{dN_\gamma}{dt d\omega} \Big|_{\text{em}}^{\text{K,rel}} = \frac{2\sqrt{2}\alpha Z^2}{\sqrt{3}\pi\theta_e} \frac{N_e N_i \sigma_{\text{TC}}}{\omega} e^{-\omega/\theta_e} I(\omega, \theta_e) \quad (19a)$$

$$\begin{aligned} I(\omega, \theta_e) &= \sqrt{\frac{\pi\theta_e}{2}} e^{\omega/\theta_e} \int_{p_{\text{min}}}^{\infty} p_1 \gamma_1 f(p_1) dp_1 \\ &= \sqrt{\frac{\pi\theta_e}{2}} \frac{e^{-1/\theta_e}}{K_2(1/\theta_e)} \left[(1+\omega)^2 + 2\theta_e(1+\omega) + 2\theta_e^2 \right] \\ &\approx (1+\omega)^2 \left[1 + \left(\frac{2}{1+\omega} - \frac{15}{8} \right) \theta_e \right]. \end{aligned} \quad (19b)$$

This shows that in the classical treatment the improved asymptotic scales as $\propto (1+\omega)^2 e^{-\omega/\theta_e}$ for low temperatures. The origin of this correction is not quantum-mechanical but simply due to special relativistic effects. This modification absorbs the leading order corrections towards the BH limit, as we discuss next. We also mention that in Eq. (19) the temperature-dependent factor,

$$\begin{aligned} \mathcal{R}(\theta_e) &= \sqrt{\frac{\pi\theta_e}{2}} \frac{e^{-1/\theta_e}}{K_2(1/\theta_e)} \equiv \frac{\int_0^\infty p^2 e^{-p^2/2\theta_e} dp}{\int_0^\infty p^2 e^{-(\gamma-1)/\theta_e} dp} \\ &\approx 1 - \frac{15}{8}\theta_e + \frac{345}{128}\theta_e^2 - \frac{3285}{1024}\theta_e^3, \end{aligned} \quad (20)$$

is directly related to the differences in the normalization of the non-relativistic and relativistic Maxwell-Boltzmann distribution. At high temperatures, the corrections can become sizable, giving $\mathcal{R}(\theta_e) \approx 0.98$ at $kT_e = 5$ keV and $\mathcal{R}(\theta_e) \approx 0.84$ at $kT_e \approx 50$ keV, and thus should be taken into account for accurate calculations.

⁹ The relativistic Maxwell-Boltzmann distribution is defined with the normalization $\int p^2 f_{\text{rMB}}(p) dp = 1$.

4.2 Definition of thermally-averaged Gaunt factors

The main quantity that enters the BR emission term in the photon Boltzmann equation as well as the electron temperature evolution equation, is the thermally-averaged Gaunt factor. It can be simply obtained by comparing the total plasma emissivity with the emissivity in the Kramers limit and is usually computed as

$$\begin{aligned}\bar{g}(\omega, \theta_e) &= \frac{\int_{p_{\min}}^{\infty} \frac{p_1^3}{\gamma_1} f(p_1) \left. \frac{d\sigma(\omega, p_1)}{d\omega} \right|_K g(\omega, p_1) dp_1}{\int_{p_{\min}}^{\infty} \frac{p_1^3}{\gamma_1} f(p_1) \left. \frac{d\sigma(\omega, p_1)}{d\omega} \right|_K dp_1} \\ &= \frac{\int_{p_{\min}}^{\infty} \frac{p_1}{\gamma_1} f(p_1) g(\omega, p_1) dp_1}{\int_{p_{\min}}^{\infty} \frac{p_1}{\gamma_1} f(p_1) dp_1} \\ &\equiv \int_0^{\infty} e^{-\xi} g(\omega, p_1 = \sqrt{(\omega + \theta_e \xi)(2 + \omega + \theta_e \xi)}) d\xi. \quad (21)\end{aligned}$$

In the last step we explicitly assumed that the electrons follow a non-degenerate, relativistic Maxwell-Boltzmann distribution¹⁰.

In the non-relativistic limit ($\gamma_1 \approx 1$), Eq. (21) is a very good choice. However, for $p_1 \gtrsim 1$, the Gaunt factor scales $\propto \gamma_1^2$ at low frequencies (see Sect. 2.3). It is thus useful to multiply the Kramers cross section by γ_1^2 , which then yields a slightly modified definition for the Bremsstrahlung Gaunt factor:

$$\begin{aligned}\bar{g}^{\text{rel}}(\omega, \theta_e) &= \frac{\int_{p_{\min}}^{\infty} p_1 \gamma_1 f(p_1) g^{\text{rel}}(\omega, p_1) dp_1}{\int_{p_{\min}}^{\infty} p_1 \gamma_1 f(p_1) dp_1} \\ &= \frac{\int_{p_{\min}}^{\infty} \frac{p_1}{\gamma_1} f(p_1) dp_1}{\int_{p_{\min}}^{\infty} p_1 \gamma_1 f(p_1) dp_1} \bar{g}(\omega, \theta_e) \\ &\equiv \frac{\bar{g}(\omega, \theta_e)}{(1 + \omega)^2 + 2(1 + \omega)\theta_e + 2\theta_e^2} \\ g^{\text{rel}}(\omega, p_1) &= \gamma_1^{-2} g(\omega, p_1). \quad (22)\end{aligned}$$

This redefinition reduces the dynamic range of the Gaunt factor and is thus very useful for compressing the data in tabulations. The final Bremsstrahlung emission term then takes the form

$$\left. \frac{dN_\gamma}{dt d\omega} \right|_{\text{em}} = \frac{2\sqrt{2}\alpha Z^2}{\sqrt{3\pi\theta_e}} \frac{N_e N_i \sigma_{\text{TC}}}{\omega} e^{-\omega/\theta_e} I(\omega, \theta_e) \bar{g}^{\text{rel}}(\omega, \theta_e) \quad (23a)$$

$$= \frac{2\sqrt{2}\alpha Z^2}{\sqrt{3\pi\theta_e}} \frac{N_e N_i \sigma_{\text{TC}}}{\omega} e^{-\omega/\theta_e} \mathcal{R}(\theta_e) \bar{g}(\omega, \theta_e), \quad (23b)$$

where $I(\omega, \theta_e)$ given by Eq. (19b) and $\mathcal{R}(\theta_e)$ by Eq. (20). Both definitions of course give exactly the same answer for the overall Bremsstrahlung emission term. Nevertheless, in applications $\bar{g}^{\text{rel}}(\omega, \theta_e)$ is beneficial since it does not scale as strongly with temperature and can also be extrapolated towards high photon energies without further computation (see discussion below).

4.3 Thermally-averaged NR and BH Gaunt factors

In this section we illustrate the effects of thermal averaging on the non-relativistic and Bethe-Heitler Gaunt factors. We also consider the improvements by adding a factor of γ_1^2 to the Kramers' and NR formulae to capture the main relativistic correction. This leads to a more moderate scaling of the Gaunt factor at high frequencies and also improves the agreement with the EH result.

¹⁰ We have $\int_{p_{\min}}^{\infty} \frac{p_1}{\gamma_1} f(p_1) dp_1 = \int_{p_{\min}}^{\infty} \frac{p_1}{\gamma_1} f(p_1) dp_1 = e^{-(1+\omega)/\theta_e} / K_2(1/\theta_e)$ in this case, which cancels a corresponding factor from the numerator.

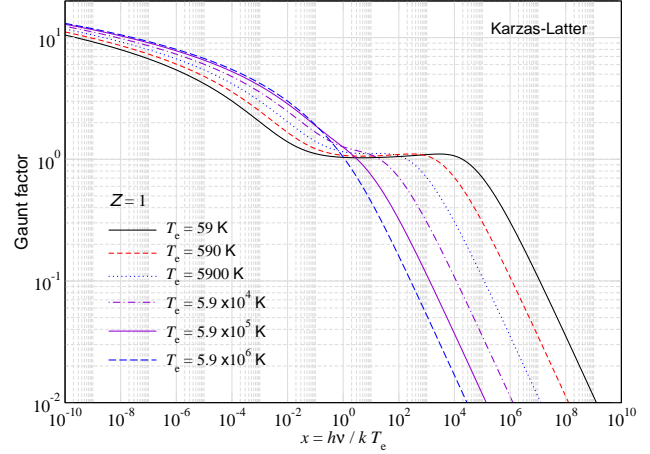


Figure 10. Thermally-averaged Gaunt factor with definitions as in KL for $Z = 1$ (see Sect. 4.3.1 for details). The steep drop at high photon energies is because relativistic boosting is not accounted for, an effect that is cured by our modified non-relativistic expression (see Fig. 11 and 15).

4.3.1 Karzas-Latter case

We start our discussion by reproducing the results from KL for the non-relativistic Gaunt factor. Similar figures can also be found in van Hoof et al. (2014). To obtain this result we need to use $\eta_i^{\text{KL}} = \alpha Z/p_i$ instead of $\eta_i = \alpha Z \gamma_i/p_i$ in Eq. (2). We furthermore approximate the relative speed by $|v_{\text{rel}}| \approx p_1$ and assume a non-relativistic Maxwellian, $f_{\text{nr}}(p) = \sqrt{2/\pi} \theta_e^{-3/2} e^{-p^2/2\theta_e}$. The minimal momentum is furthermore set to $p_{\min} \approx \sqrt{2\omega}$. With this the Gaunt factor's thermal average, Eq. (21), reduces to

$$\begin{aligned}\bar{g}^{\text{KL}}(\omega, \theta_e) &= \frac{\int_{\sqrt{2\omega}}^{\infty} p_1 e^{-p_1^2/2\theta_e} g^{\text{KL}}(\omega, p_1) dp_1}{\int_{\sqrt{2\omega}}^{\infty} p_1 e^{-p_1^2/2\theta_e} dp_1} \\ &= \frac{\int_{\omega/\theta_e}^{\infty} e^{-\xi} g^{\text{KL}}(\omega, p_1 = \sqrt{2\theta_e \xi}) d\xi}{\int_{\omega/\theta_e}^{\infty} e^{-\xi} d\xi} \\ &\equiv \int_0^{\infty} e^{-\xi} g^{\text{KL}}(\omega, p_1 = \sqrt{2(\omega + \theta_e \xi)}) d\xi, \quad (24)\end{aligned}$$

which is equivalent to Eq. (21) of KL after switching to the absorption Gaunt factor (exchange of the roles of the incoming and outgoing electrons and use of energy conservation). It also directly follows from Eq. (21) for $\theta_e, \omega \ll 1$.

Figure 10 illustrates the thermally-averaged Gaunt factor for varying temperature and $Z = 1$ using the approximations of KL. At high photon energies, a steep drop of the Gaunt factor is observed. This is not found for the EH result even at these relatively low temperatures and is simply caused by the fact that in the tail of the electron distribution function relativistic correction cannot be neglected. By switching back to $\eta_i = \alpha Z \gamma_i/p_i$ instead of $\eta_i^{\text{KL}} = \alpha Z/p_i$ and inserting this into Eq. (21) [i.e., not setting factors of γ_i to unity], we obtain the results in Fig. 11. The unphysical drop of the Gaunt factor at high energies is removed by this transformation and the Gaunt factor become constant at $x = \omega/\theta_e \gtrsim 3/\theta_e$ or $h\nu \gtrsim 3m_e c^2$. Although this already is an improvement of the non-relativistic expression, it still underestimates the result at high frequencies. However, the Gaunt factor can now be extrapolated to any higher frequency using a finite range in x . Another improvement can be achieved by adding a factor of γ_1^2 to the NR cross section, as will be discussed below (see Fig. 15).

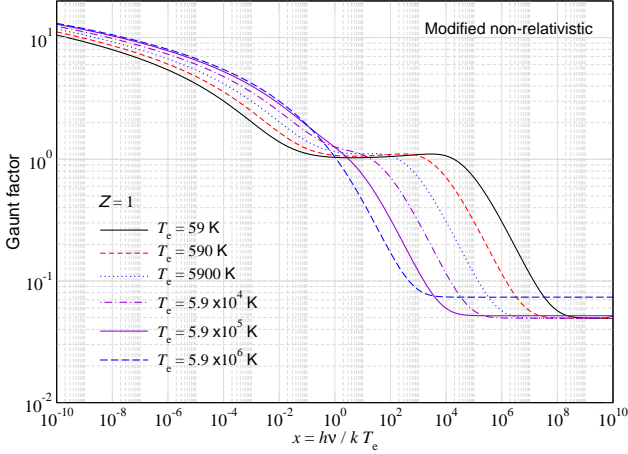


Figure 11. Thermally-averaged Gaunt factor in the non-relativistic limit [Eq. (2)] for $Z = 1$ when using the standard definition, Eq. (21), for the thermal average. The replacement of $\eta_i^{\text{KL}} = \alpha Z/p_i$ by $\eta_i = \alpha Z\gamma_i/p_i$ removes the unphysical drop of the KL Gaunt factor at high energies (cp. Fig. 10).

4.3.2 Bethe-Heitler case

To illustrate the BH case, we first use Eq. (7) in Eq. (21), obtaining the results presented in Fig. 12. In this case, our results are in very good agreement with those obtained by Nozawa et al. (1998) and van Hoof et al. (2015). The BH Gaunt factor shows a steep increase towards high frequencies. At temperature $T_e \gtrsim 5.9 \times 10^8$ K ($\theta_e \gtrsim 0.1$), an additional increase of the overall Gaunt factor amplitude by $\approx \langle \gamma_1^2 \rangle \approx 1 + 3\theta_e + 15\theta_e^2/2$ furthermore becomes noticeable. Both aspects can be avoided by using the relativistically-improved Kramers cross section for reference. This approach is taken for our modified thermal average, Eq. (22), and illustrated in Fig. (13). The modification captures the main relativistic effects and greatly reduces the dynamic range of the Gaunt factors, which is beneficial for numerical applications. Again, extrapolation of the Gaunt factor to very high energies is possible using a finite range in x , since $\bar{g}^{\text{rel}}(\omega, \theta_e)$ becomes roughly constant at $x = \omega/\theta_e \gtrsim 3/\theta_e$ or $h\nu \gtrsim 3m_e c^2$. In BRpack, we make use of this property.

4.4 Thermally-averaged Gaunt factor for the EH case

We are now in the position to compute the thermally-averaged EH Gaunt factor. In Fig. 14 we illustrate the results over a wide range of temperatures and photon energies. We directly used our modified definition for the thermal average, Eq. (22), which greatly reduces the dynamic range. This definition is ideal for tabulation of the result, and is used in BRpack. At high photon energies the result can be obtained by extrapolation, however, the net emission vanishes in this limit for any practical purposes. To our knowledge, this is the first precise representation of the thermally-averaged EH Gaunt factor for hydrogen over an as vast range of energies. Cases for $Z \leq 10$ can also be quickly computed using BRpack.

4.4.1 Comparison with simple approximations

We now compare the various approximations for the thermally-averaged Gaunt factor with the those obtained from the EH expressions. For electron temperature $T_e = 5.9 \times 10^4$ K ($\theta_e = 10^{-5}$) and $Z = 1$ the results are shown in Fig. 15, using the standard definition for the Gaunt factor thermal average, Eq. (21). As expected, the

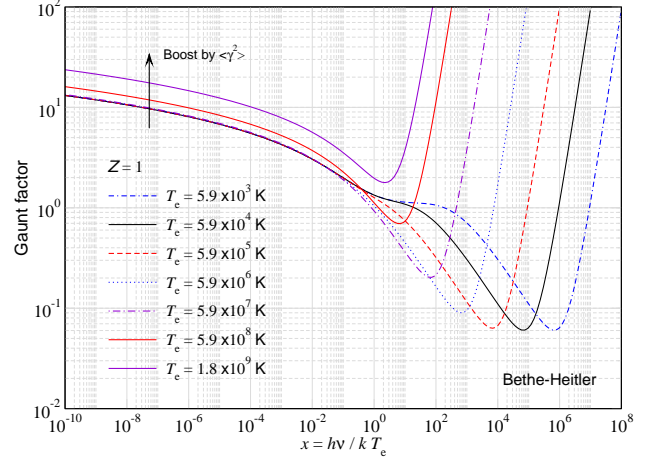


Figure 12. Thermally-averaged relativistic BH Gaunt factor for $Z = 1$ and varying temperature ($\theta_e = \{10^{-6}, 10^{-5}, 10^{-4}, 10^{-3}, 10^{-2}, 0.1, 0.3\}$). The BH Gaunt factor exhibits a steep increase at high frequencies. At temperature $T_e \gtrsim 5.9 \times 10^8$ K ($\theta_e \gtrsim 0.1$), extra boosting by $\approx \langle \gamma_1^2 \rangle$ becomes relevant. Both aspects can be captured by redefining the thermal average (see Fig. 13), which reduces the dynamic range of the Gaunt factors.

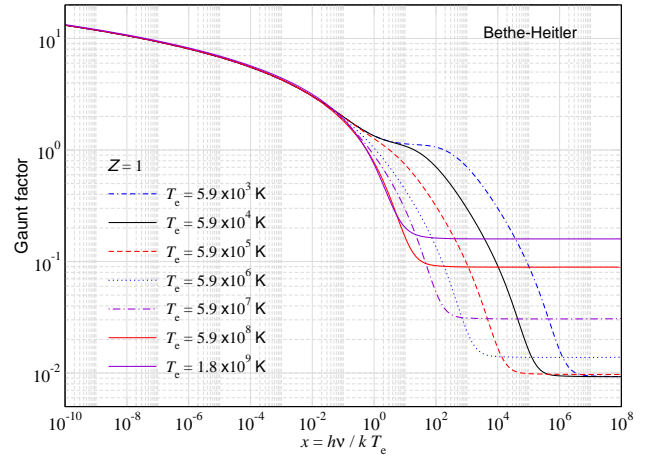


Figure 13. Same as in Fig. 12 but using our modified definition for the thermal average, Eq. (22). The dynamic range is greatly reduced by the redefinition of the thermal average.

Bethe-Heitler approximation works extremely well at high frequencies, where all contributions indeed arise from relativistic electrons of the Maxwellian. In contrast, the NR expressions work very well at low frequencies. As already shown in Sect. 3.3, the agreement with the EH result can be further improved by multiplying the cross section by a factor of γ_1^2 , which captures the main relativistic boosting effect. The overall scaling of the EH result is well-represented by our improved non-relativistic expression given in Eq. (6).

4.4.2 Domains of validity

For a more quantitative accuracy assessment of the NR and BH formula, we again perform a comparison similar to the one discussed in Sect. 3.3. We compute the thermally-averaged Gaunt factor using solely the BH formula or the NR expression and then ask for which pairs (x, θ_e) it deviates from the one obtained us-

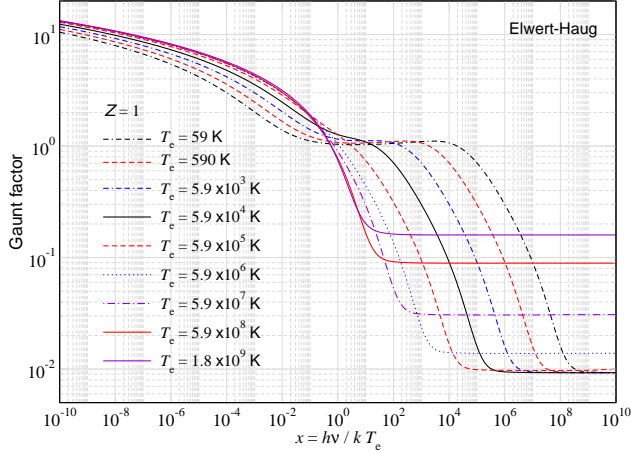


Figure 14. Thermally-averaged Gaunt factor using the integrated expressions of EH in Eq. (22) for $Z = 1$ and varying temperature (corresponding to $\theta_e = \{10^{-8}, 10^{-7}, 10^{-6}, 10^{-5}, 10^{-4}, 10^{-3}, 10^{-2}, 0.1, 0.3\}$).

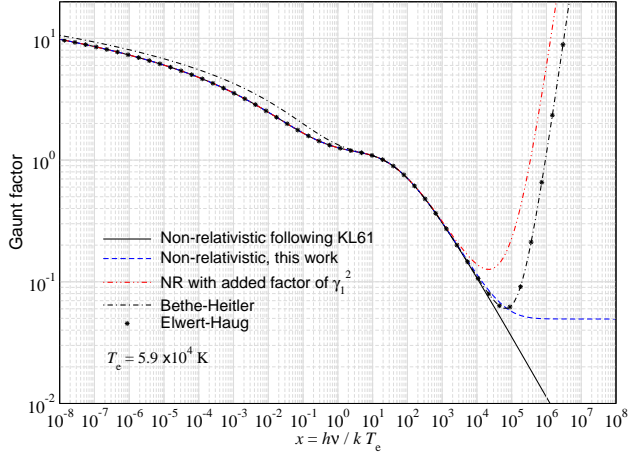


Figure 15. Thermally-averaged Gaunt factors for $Z = 1$ when using the standard definition, Eq. (21), for the thermal average and various limits for the cross section. The EH result is shown for comparison. BH works very well at high photon energies, while the non-relativistic expressions capture the behavior at low energies. An improvement of the non-relativistic expression is obtained when adding a factor of γ_1^2 .

ing EH by less than a given threshold. The corresponding regions for $Z = 1$ and $Z = 2$ are displayed in Fig. 16, in red for the NR approximation and in blue for the BH formula. From top to bottom the required agreement is at least 0.3%, 1%, and 1%. Some caveats about the BH validity region should be mentioned here. Due to the structured behavior of the averaged Gaunt factor (cf. Fig. 15), several disconnected regions are identified as valid when using the described thresholding procedure, especially for high-accuracy thresholds. We thus only highlight the points (x, θ_e) such that $(\tilde{x}, \theta_e) \in \text{BH validity region}$ for all $\tilde{x} \geq x$. Overall we find that a combination of the BH and NR expressions for $Z \lesssim 10$ leads to a good description of the full EH Gaunt-factor over a wide range of photon energies and electron temperatures unless precision $\lesssim 1\%$ is required. For $Z = 1$ and 2, we expect BRPACK to provide a better than 0.03% level representation of the thermally-averaged EH Gaunt factor at all photon energies. In particular the low-frequency

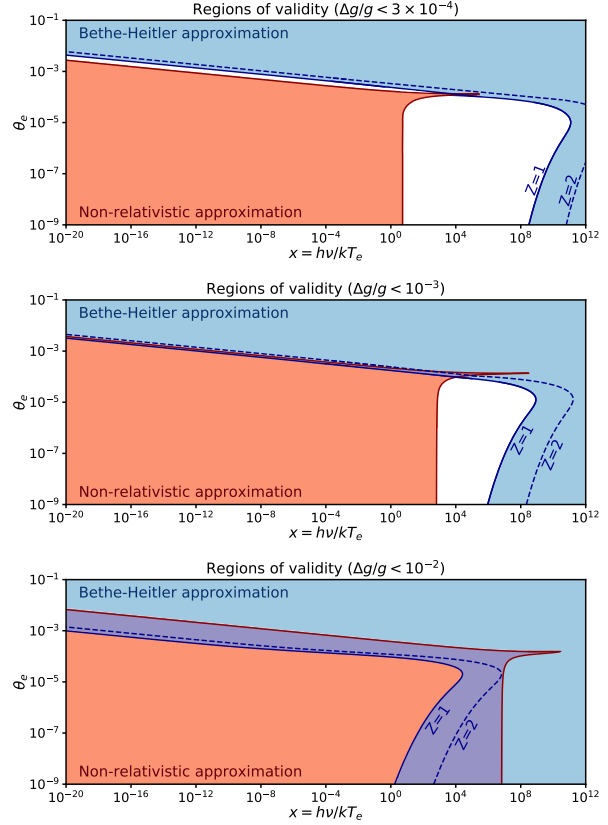


Figure 16. Regions in which the NR and BH approximations can be used to calculate the thermally-averaged Gaunt factor. The colored areas show the (x, θ_e) domains where the relative difference with respect to the thermally-averaged EH Gaunt factor is 0.3% (Top panel), 1% (Middle panel), or 1% (Bottom panel) for $Z = 1$. The dashed line displays the boundary of the BH region for $Z = 2$. The NR regions for $Z = 1$ and 2 coincide at the plot resolution. In the white areas, the EH formula is required.

part of the EH emission spectrum should be represented very accurately up to mildly-relativistic temperatures $kT_e \approx 50 \text{ keV}$.

We also note that since for $Z \leq 10$ we only tabulated the EH Gaunt-factor up to $p_1 = 2$, at $x \gtrsim 1.2/\theta_e$, we always switch to the BH result. The error with respect to the full EH evaluation should be limited to $\lesssim 0.5\%$ (see Fig. 9), which again should not cause any severe limitations for astrophysical applications at $\theta_e \lesssim 0.1$.

4.5 Comparison with previous works

The thermally-averaged Gaunt factor for the cross section expressions of KL and Bethe-Heitler formula were previously considered in detail (Itoh et al. 1985; Nozawa et al. 1998; Itoh & et. al. 2000; van Hoof et al. 2014, 2015). For the non-relativistic regime, the KL definition for the thermally-average Gaunt factor, Eq. (24), was used. For the BH limit, the Gaunt factor definition of the aforementioned works relates to ours, Eq. (21), by

$$\bar{g}^{\text{Itoh}}(\omega, \theta_e) = \mathcal{R}(\theta_e) \bar{g}(\omega, \theta_e). \quad (25a)$$

In Itoh & et. al. (2000), fits were given over a limited range of photon energies and temperatures, while van Hoof et al. (2014, 2015) provided extensive tables covering a wide range of temperatures, photon energies and ion charges Z . We were able to reproduce the results of van Hoof et al. (2014, 2015) for the KL and BH limits,

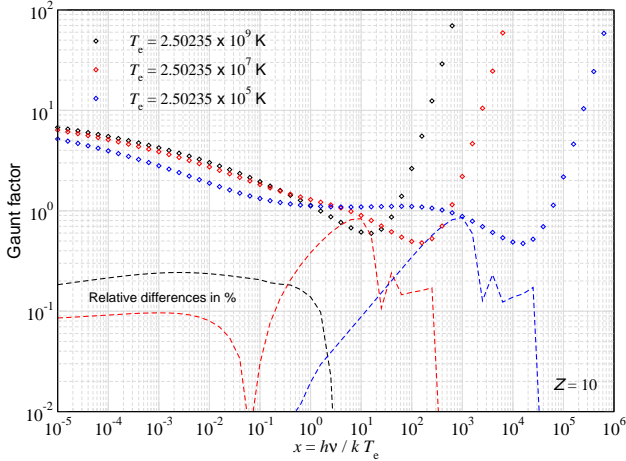


Figure 17. Direct comparison of the EH Gaunt factor with the values given by van Hoof et al. (2015) for $Z = 10$. The dashed lines show the relative differences in percent. At $x \approx 1 - 10^3$, the departures can reach the percent level at low and intermediate temperatures. The abrupt drop of the relative differences (absolute value) at high frequencies are due to our limited tables of the total EH Gaunt factor (see text for explanation).

finding excellent agreement. We also confirmed the results of Itoh & et. al. (2000) at $x = 10^{-4} - 20$ finding very good agreement.

In van Hoof et al. (2015), the KL and BH limits were ‘merged’ to mimic the transition between the non-relativistic and relativistic regimes. However, no explicit assessment of the accuracy of this procedure was provided. As we saw in Sec. 3.3, for low ion charge $Z \leq 10$ we can expect departures to become visible at the level of 0.1 – 1%. For $Z = 1$ and $Z = 2$, we find the EH calculation to agree with van Hoof et al. (2015) at the 0.1% level, while for higher charges the differences do exceed this level. Again, this outcome is expected given the discussion of Sect. 3.3.

In Fig. (17), we show our result for the EH Gaunt factor and relative difference with respect to van Hoof et al. (2015) for several temperatures and ion charge $Z = 10$. For the comparison, we took the exact values from the tables provided by van Hoof et al. (2015) without any interpolation. The departures are visible at the $\approx 0.1 - 1\%$ level around $x \approx 1 - 10^4$ and low temperatures, $\theta_e \lesssim 0.01$. We also see an abrupt drop in the relative difference around $x \approx 3$, $x \approx 300$ and 3×10^4 for the three shown cases. This is because our tables for the EH Gaunt factor only extend up to $p_1 = 2$, such that at very high photon energies we always converge to the BH result, and thus agree with van Hoof et al. (2015) to high precision. Note however, that at these high photon energies hardly any BR emission is expected such that errors should remain minor for astrophysical applications. The low-frequency region is much more crucial in this respect and we expect our thermally-averaged Gaunt factor to be highly accurate there ($\Delta g/g \lesssim 0.1\%$ at $x \lesssim 1$ for $Z \leq 10$).

For larger values of Z , the departures exceed the percent-level. We numerically evaluated the case $Z = 20$ finding differences with respect to van Hoof et al. (2015) at the level of $\approx 2 - 3\%$ around $x \approx 1 - 10^4$ and temperatures $\theta_e \lesssim 0.01$. However, for higher ionic charge also additional Coulomb corrections and shielding effects should also be accounted for, such that we leave a more quantitative comparison to future work. BRpack should yield reliable results for $Z \leq 10$ and $\theta_e \lesssim 0.1$ at $\lesssim 0.5\%$ precision. For $Z \leq 4$, the EH Gaunt factor should be reproduced at the level of $\lesssim 0.1\%$ precision.

5 CONCLUSION

We presented a comprehensive study of the free-free Gaunt factor, $g(\omega, p_1)$, and its thermally-averaged version, which is relevant to many astrophysical applications. Our focus was on ions with low ionic charge ($Z \leq 10$), for which we computed the BR Gaunt factors using the differential cross section expressions given by EH. We compared our results with various approximations and previous Gaunt factor computations, illustrating the domains of validity and their precision (e.g., Fig. 5). Our results for $g_{\text{EH}}(\omega, p_1)$ should be accurate at the level of $\lesssim 0.03\%$ for $Z \leq 10$ and $p_1 \leq 2$. For the thermally-averaged EH Gaunt factor we expect our computations to yield $\lesssim 0.1\%$ precision at $kT_e \lesssim 50$ keV for $Z \leq 4$ and slightly better ($\Delta g/g \lesssim 0.03\%$) for $Z \leq 2$. For $Z \leq 10$ we expect an overall precision of $\lesssim 0.5\%$ for the thermally-averaged EH Gaunt factor at temperatures $kT_e \lesssim 50$ keV.

We simplified the computations of the EH differential cross section, showing that the hypergeometric function evaluations can be reduced to an evaluation of one real function. This function can be computed using an ordinary differential equation and thus improves the computational precision and efficiency greatly. In a similar manner we showed that the non-relativistic Gaunt factor can also be related to the same real function [see Eq. (3)]. Overall, our numerical procedure allow us to precisely compute the EH Gaunt factor over a wide range of energies, with extensions to low and high photon energies obtained using analytic expressions. Coulomb corrections and shielding effects are expected to become important for $Z > 10$ and at high electron energies. These can in principle be added using our computational method.

We developed new software package, BRpack, which allows efficient and accurate representation of the NR, BH and EH Gaunt factors for $Z \leq 10$, both for individual values of the electron and photon momenta as well as for thermally-averaged cases. It should prove useful for computations of CMB spectral distortions and radiative transfer problems in the intergalactic medium at low redshifts. We can furthermore use the Gaunt factor for improved modeling of the free-free emission from our own galaxy, potentially even taking non-thermal contributions into account without mayor complications. Our procedure can also be applied to computations of the e^-e^- and e^-e^+ Bremsstrahlung processes (e.g., Haug 1985, 1975; Itoh et al. 2002), which will be important at higher plasma temperatures ($kT_e/m_e c^2 \gtrsim 1$).

While with BRpack a numerical precision of better than $\approx 0.01\%$ can be reached for any photon and electron energy, it is clear that this does not fully reflect the accuracy of the Gaunt factor. Higher order Coulomb corrections, shielding effects and radiative corrections are not accounted for by the EH expression. These invalidate the cross section at higher energies and for large ion charge (Tseng & Pratt 1971; Roche et al. 1972; Haug 2008). However, even at the temperatures and photon energies of interest to us ($kT_e \lesssim \text{few} \times \text{keV}$), corrections may become relevant at $\lesssim 0.1\%$ accuracy. In this case, exact calculations using Dirac-wave functions (e.g., Tseng & Pratt 1971; Pořkus 2018, 2019) for the electron may be required. Given the many applications of the BR process in astrophysics, accurate calculations with the goal to provide comprehensive, user-friendly, quasi-exact representations of the process for a wide range of conditions should be undertaken. We look forward to further investigations of the problem.

Acknowledgments: This work was supported by the ERC Consolidator Grant *CMBSPEC* (No. 725456) as part of the European Union’s Horizon 2020 research and innovation program. JC was supported by the Royal Society as a Royal Society URF at the University of Manchester, UK.

APPENDIX A: PROPERTIES OF G_ℓ

We first prove that G_ℓ is real. Starting from Eq. (2b), this can be seen with

$$\begin{aligned} G_\ell^*(\eta_1, \eta_2, x) &= (-x)^{\ell+1} (1-x)^{-\frac{i(\eta_1+\eta_2)}{2}} e^{-\pi\eta_1} \\ &\quad {}_2F_1(1+\ell-i\eta_1, 1+\ell-i\eta_2, 2\ell+2, x) \\ &= (-x)^{\ell+1} (1-x)^{-\frac{i(\eta_1+\eta_2)}{2}} (1-x)^{i(\eta_1+\eta_2)} e^{-\pi\eta_1} \\ &\quad {}_2F_1(1+\ell+i\eta_1, 1+\ell+i\eta_2, 2\ell+2, x) \\ &\equiv G_\ell(\eta_1, \eta_2, x), \end{aligned} \quad (\text{A1})$$

where we used ${}_2F_1(a, b, c, x) = (1-x)^{c-a-b} {}_2F_1(c-a, c-b, c, x)$ for the hypergeometric function. More generally one can show that

$$f(x)(1-x)^{\frac{\pm i(a+b)}{2}} {}_2F_1(c \pm ia, c \pm ib, 2c, x) \quad (\text{A2})$$

$$f(x)(1-x)^{\frac{\pm i(a-b)}{2}} {}_2F_1(c \pm ia, c \mp ib, 2c, x) \quad (\text{A3})$$

are all real functions for real a, b, c and x . These relations are very useful when studying recurrence relations for G_ℓ (Appendix A3). In particular it is beneficial to include $f(x) = \sqrt{1-x}$ in the definition of $G_\ell(x)$.

A1 Relation between G_0 and G_1

To simplify the computation of the non-relativistic Gaunt factor it is useful to study the relation between G_0 and G_1 . The hypergeometric function related to $G_\ell(x)$ are $F_\ell(x) = {}_2F_1(1+\ell+i\eta_1, 1+\ell+i\eta_2, 2(\ell+1), x)$. Taking the first and second derivatives of F_0 with respect to x , we find

$$\begin{aligned} F_0' &= \frac{1}{2}(1+i\eta_1)(1+i\eta_2){}_2F_1(2+i\eta_1, 2+i\eta_2, 3, x) \\ &= \frac{1}{2}(1+i\eta_1)(1+i\eta_2)(1-x)^{-1-i\eta_+} {}_2F_1(1-i\eta_1, 1-i\eta_2, 3, x) \quad (\text{A4a}) \end{aligned}$$

$$= \left[G_0' - \left(\frac{1}{x} - \frac{i\eta_+}{2(1-x)} \right) G_0 \right] e^{\pi\eta_1} \frac{(1-x)^{-i\frac{\eta_+}{2}}}{(-x)} \quad (\text{A4b})$$

$$F_0'' = \frac{1+i\eta_+}{1-x} F_0' + \frac{(1+\eta_1^2)(1+\eta_2^2)}{6(1-x)} F_1 \quad (\text{A4c})$$

with $\eta_\pm = \eta_1 \pm \eta_2$. For the differential equation of F_0 we have

$$x(1-x)F_0'' + [2-(3+i\eta_+)x]F_0' - (1+i\eta_1)(1+i\eta_2)F_0 = 0.$$

Inserting Eq. (A4c) then yields

$$\frac{(1+\eta_1^2)(1+\eta_2^2)}{6} xF_1 + 2(1-x)F_0' - (1+i\eta_1)(1+i\eta_2)F_0 = 0.$$

Multiplying this equation by $G_0/F_0 = (-x)(1-x)^{\frac{i\eta_+}{2}} e^{-\pi\eta_1}$ and combining with Eq. (A4b), we then obtain

$$\begin{aligned} & - \frac{(1+\eta_1^2)(1+\eta_2^2)}{6} G_1 + 2(1-x)G_0' - \left[\frac{2}{x} - 2 - i\eta_+ + (1+i\eta_1)(1+i\eta_2) \right] G_0 \\ &= - \frac{(1+\eta_1^2)(1+\eta_2^2)}{6} G_1 + 2(1-x)G_0' + \left[\eta_1\eta_2 + \frac{1}{2} \left(\frac{\eta_1}{\eta_2} + \frac{\eta_2}{\eta_1} \right) \right] G_0 = 0. \\ &\longleftrightarrow G_0' = \left[\eta_1\eta_2 + \frac{1}{2} \left(\frac{\eta_1}{\eta_2} + \frac{\eta_2}{\eta_1} \right) \right] G_0 - \frac{(1+\eta_1^2)(1+\eta_2^2)}{6} G_1 \quad (\text{A5}) \end{aligned}$$

By comparing with Eq. (2), we can thus obtain Eq. (3).

A2 Differential equation for G_0

Since G_0 and G_0' are both real functions it is useful to study the associated differential equation directly. From the differential equation for the hypergeometric function F_0 we find

$$x(1-x)^2 G_0'' - x(1-x)G_0' + \left[\eta_1\eta_2 + \frac{\eta_-^2}{4}x \right] G_0 = 0. \quad (\text{A6})$$

This can be converted into a set of first order equations

$$G_0' = H_0 \quad (\text{A7a})$$

$$H_0' = \frac{H_0}{1-x} - \left[\frac{\eta_1\eta_2}{x} + \frac{\eta_-^2}{4} \right] \frac{G_0}{(1-x)^2}. \quad (\text{A7b})$$

This system has regular singular points at $x = 0, 1, \infty$. For our problems we need the solution at $x < 0$. Choosing a starting point very close to the

origin, convenient initial conditions are

$$G_0(x) \approx -e^{-\pi\eta_1} x \left[1 + \frac{x}{2}(1-\eta_1\eta_2) \right] \quad (\text{A8a})$$

$$H_0(0) = G_0'(0) \approx -e^{-\pi\eta_1} [1 - x(1-\eta_1\eta_2)]. \quad (\text{A8b})$$

These allow solving the problem for various values of η_1 and η_2 of interest using a solver based on the Gear's method (Chluba et al. 2010). Due to the factor $e^{-\pi\eta_1}$, this procedure is limited to $p_1 \gtrsim 8 \times 10^{-5} Z$. At lower values of p_1 , we can start with rescaled initial conditions and then reinitialize the solver after appropriate intervals multiplying portions of $e^{-\pi\eta_1}$. For required values of x , this leads to numerically stable results.

A3 Recursion relation for G_ℓ

Here we briefly rederive recurrence relations for G_ℓ following a procedure that is similar to that of Karzas & Latter (1961); Hummer (1988). The same relations are useful for the EH cross section computation, as we show below. The starting point is

$$\begin{aligned} G_\ell(x) &= (-x)^{\ell+1} (1-x)^{\frac{i\eta_+}{2}} e^{-\pi\eta_1} \\ &\quad {}_2F_1(1+\ell+i\eta_1, 1+\ell+i\eta_2, 2(\ell+1), x), \end{aligned} \quad (\text{A9})$$

with $\eta_\pm = \eta_1 \pm \eta_2$. To obtain the recurrence relations one expresses ${}_2F_1$ in terms of G_ℓ . We first define¹¹ $\tilde{G}_\ell = \sqrt{1-x} G_\ell$ and then write

$$F_\ell(x) = \tilde{G}_\ell(x) (-x)^{-(\ell+1)} (1-x)^{-\frac{i\eta_+}{2} - \frac{1}{2}} e^{\pi\eta_1}. \quad (\text{A10})$$

This can then be inserted into the differential equation for the hypergeometric functions (which $F_\ell(x)$ fulfills), yielding

$$x^2(1-x)^2 \tilde{G}_\ell''(x) = \left\{ \ell(\ell+1) - [\eta_1\eta_2 + \ell(\ell+1)]x - \frac{1+\eta_-^2}{4}x^2 \right\} \tilde{G}_\ell(x).$$

In the evaluation of the non-relativistic cross section, we always have $x < 0$. Assuming $|x| < 1/2$, one can use the Ansatz $\tilde{G}_\ell(x) = (-x)^{\ell+1} e^{-\pi\eta_1} \sum_n a_n x^n$, which yields

$$\begin{aligned} a_0 &= 1, \quad a_1 = \frac{\ell(\ell+1) - \eta_1\eta_2}{2\ell+2} \\ a_n &= (\kappa_{n\ell} - \lambda_{n\ell}) a_{n-1} - (\mu_{n\ell} + \nu_{n\ell}) a_{n-2} \\ \kappa_{n\ell} &= \frac{\ell(\ell+1) + 2(n-1)(2\ell+n)}{n(2\ell+1+n)}, \quad \lambda_{n\ell} = \frac{\eta_1\eta_2}{n(2\ell+1+n)}, \\ \mu_{n\ell} &= \frac{[2(\ell+n)-3]^2}{4n(2\ell+1+n)}, \quad \nu_{n\ell} = \frac{(\eta_1-\eta_2)^2}{4n(2\ell+1+n)} \end{aligned} \quad (\text{A11})$$

for the coefficients, and thus $G_\ell(x) = (-x)^{\ell+1} e^{-\pi\eta_1} \sum_n a_n x^n / \sqrt{1-x}$.

Hummer (1988) directly evaluated $a_n = a_n x^n$, however, in our applications we also evaluate G_ℓ for varying x at fixed values of η_1 and η_2 . In this case it is better to store the required values of a_n instead. The real gains are marginal in any case, in particular since for the evaluation of the sum one can compute $x^n = x(x^{n-1})$ in each step at hardly any extra cost. We also did not find the stability of the expressions to improve by changing the procedure. Stability issues could be solved using arbitrary number precision or resorting to the differential equation for G_0 .

For $-2 < x < -1/2$, to accelerate convergence one should rewrite the expressions in terms of $y = x/(x-1)$, which maps the interval into $1/3 < y < 2/3$. Applying hypergeometric function relations, we find

$$\begin{aligned} G_\ell(y) &= y^{\ell+1} (1-y)^{\frac{i\eta_-}{2}} e^{-\pi\eta_1} \\ &\quad {}_2F_1(1+\ell+i\eta_1, 1+\ell-i\eta_2, 2\ell+2, y) \end{aligned} \quad (\text{A12a})$$

$$F_\ell(y) = \tilde{G}_\ell(y) (-y)^{-(\ell+1)} (1-y)^{-\frac{i\eta_-}{2} - \frac{1}{2}} e^{\pi\eta_1}. \quad (\text{A12b})$$

with $\tilde{G}_\ell(y) = (-1)^{\ell+1} \sqrt{1-y} G_\ell(y)$. Comparing with Eq. (A10), we thus can again apply the recurrence relations, Eq. (A11), for $\tilde{G}_\ell(y)$ after replacing $x \rightarrow y = x/(x-1)$ and $\eta_2 \rightarrow -\eta_2$.

To treat the problem at $x < -2$, we use $z = 1/x$, which maps the

¹¹ This reduces the number of terms.

interval into $-1/2 < z < 0$. In this case, *two* new recursions are needed. Applying the hypergeometric function relations, we can write

$$\begin{aligned}
 G_\ell(z) &= (-z)^{-(\ell+1)} [-(1-z)/z]^{\frac{\eta_+}{2}} (-z)^{\ell+1} e^{-\pi\eta_1} \\
 &\quad \times \left[(-z)^{\eta_1} \Lambda_\ell(\eta_1, \eta_2) {}_2F_1(1 + \ell + i\eta_1, i\eta_1 - \ell, 1 + i\eta_-, z) \right. \\
 &\quad \left. + (-z)^{\eta_2} \Lambda_\ell^*(\eta_1, \eta_2) {}_2F_1(1 + \ell + i\eta_2, i\eta_2 - \ell, 1 + i\eta_-, z) \right] \\
 &= (-z)^{\frac{\eta_-}{2}} \Lambda_\ell(\eta_1, \eta_2) H_\ell(\eta_1, \eta_2, z) + (-z)^{-\frac{\eta_-}{2}} \Lambda_\ell^*(\eta_1, \eta_2) H_\ell^*(\eta_1, \eta_2, z) \\
 &= 2\text{Re} \left[(-z)^{\frac{\eta_-}{2}} \Lambda_\ell(\eta_1, \eta_2) H_\ell(\eta_1, \eta_2, z) \right] \\
 &= \text{Re} [J_\ell(z)] \cos \left[\frac{\eta_-}{2} \ln(-z) \right] - \text{Im} [J_\ell(z)] \sin \left[\frac{\eta_-}{2} \ln(-z) \right] \\
 H_\ell(\eta_1, \eta_2, z) &= (1-z)^{\frac{\eta_+}{2}} {}_2F_1(1 + \ell + i\eta_1, i\eta_1 - \ell, 1 + i\eta_-, z) \\
 J_\ell(\eta_1, \eta_2, z) &= 2\Lambda_\ell(\eta_1, \eta_2) H_\ell(\eta_1, \eta_2, z) \\
 \Lambda_\ell(\eta_1, \eta_2) &= \frac{\Gamma(2\ell+2)\Gamma(-i\eta_-)e^{-\pi\eta_1}}{\Gamma(1+\ell-i\eta_1)\Gamma(1+\ell+i\eta_2)}. \tag{A13}
 \end{aligned}$$

This means that, similar to KL and H88, one can make the Ansatz

$$G_\ell(z) = A_\ell(z) \cos \left[\frac{\eta_-}{2} \ln(-z) \right] + B_\ell(z) \sin \left[\frac{\eta_-}{2} \ln(-z) \right], \tag{A14}$$

where $A_\ell(\eta_1, \eta_2, z) = \text{Re} [J_\ell(\eta_1, \eta_2, z)]$ and $B_\ell(z) = -\text{Im} [J_\ell(\eta_1, \eta_2, z)]$ can both be written as a real power series in z . We also have to rewrite the differential equation for $\tilde{G}_\ell(x)$ using $x = 1/z$, which gives

$$\begin{aligned}
 z^2(1-z)^2 \tilde{G}_\ell''(z) + 2z(1-z)^2 \tilde{G}_\ell'(z) \\
 = \left\{ \ell(\ell+1)z^2 - [\eta_1\eta_2 + \ell(\ell+1)]z - \frac{1+\eta_-^2}{4} \right\} \tilde{G}_\ell(z).
 \end{aligned}$$

Multiplying $G_\ell(z)$ this by $\sqrt{(z-1)/z}$ and inserting it into the differential equation for $\tilde{G}_\ell(z)$, we find the two equations

$$2\mathbf{a}_\ell^{(n)} \cdot \mathbf{A}_\ell^{(n)} + \eta_- \mathbf{b}^{(n)} \cdot \mathbf{B}_\ell^{(n)} = 0, \tag{A15a}$$

$$\eta_- \mathbf{b}^{(n)} \cdot \mathbf{A}_\ell^{(n)} - 2\mathbf{a}_\ell^{(n)} \cdot \mathbf{B}_\ell^{(n)} = 0, \tag{A15b}$$

$$\mathbf{a}_\ell^{(n)} = \begin{pmatrix} n^2 \\ \ell(\ell+1) - n(2n-3) - 1 + \frac{\eta_-^2 + \eta_+^2}{4} \\ -\ell(\ell+1) + n(n-3) + 2 - \frac{\eta_-^2}{4} \end{pmatrix}, \quad \mathbf{b}^{(n)} = \begin{pmatrix} 2n \\ -4n+3 \\ 2n-3 \end{pmatrix}. \tag{A15c}$$

for $\mathbf{A}_\ell^{(n)} = (A_\ell^{(n)}, A_\ell^{(n-1)}, A_\ell^{(n-2)})^T$ and similar for \mathbf{B}_ℓ . The symmetries of the coefficients imply $\mathbf{B}_\ell^{(n)}(\eta_1, \eta_2) = \mathbf{A}_\ell^{(n)}(\eta_2, \eta_1)$. This also means that the recursion relations for $\mathbf{B}_\ell^{(n)}(\eta_1, \eta_2)$ are identical to those for $\mathbf{A}_\ell^{(n)}(\eta_1, \eta_2)$ when switching $\eta_1 \leftrightarrow \eta_2$ and $\mathbf{A}_\ell^{(n)} \rightarrow \mathbf{B}_\ell^{(n)}$. Solving for $\mathbf{A}_\ell^{(n)}$ we find

$$\begin{aligned}
 \mathbf{A}_\ell^{(n)} &= \frac{1 + n(2n-3) - \ell(\ell+1) - \eta_1\eta_2 + \frac{3}{2}\eta_-^2(1-1/n)}{\eta_-^2 + n^2} \mathbf{A}_\ell^{(n-1)} \\
 &\quad - \frac{(n+\ell-1)(n-\ell-2) + \frac{3}{4}\eta_-^2(1-2/n)}{\eta_-^2 + n^2} \mathbf{A}_\ell^{(n-2)} \\
 &\quad + \eta_- \frac{2\ell(\ell+1) + 3n - 2 + \frac{1}{2}(\eta_+^2 + \eta_-^2)}{n(\eta_-^2 + n^2)} \mathbf{B}_\ell^{(n-1)} \\
 &\quad - \eta_- \frac{2\ell(\ell+1) + 3n - 4 + \frac{1}{2}\eta_-^2}{n(\eta_-^2 + n^2)} \mathbf{B}_\ell^{(n-2)} \tag{A16}
 \end{aligned}$$

The equations for $\mathbf{B}_\ell^{(n)}$ are obtained by switching variables, as mentioned above. The initial conditions are

$$\begin{aligned}
 \mathbf{A}_\ell^{(0)} &= 2\text{Re} \left[\frac{\Gamma(2\ell+2)\Gamma(-i\eta_-)e^{-\pi\eta_1}}{\Gamma(1+\ell-i\eta_1)\Gamma(1+\ell+i\eta_2)} \right] \\
 \mathbf{B}_\ell^{(0)} &= -2\text{Im} \left[\frac{\Gamma(2\ell+2)\Gamma(-i\eta_-)e^{-\pi\eta_1}}{\Gamma(1+\ell-i\eta_1)\Gamma(1+\ell+i\eta_2)} \right], \tag{A17}
 \end{aligned}$$

which both can be easily computed using standard libraries. This then gives the solutions $A_\ell(\eta_1, \eta_2, z) = \sum_n A_\ell^{(n)} z^n$ and similar for $B_\ell(\eta_1, \eta_2, z)$.

A3.1 Dealing with $\Lambda_\ell(\eta_1, \eta_2)$

To evaluate the initial conditions for the recurrence relations we need

$$\begin{aligned}
 \Lambda_\ell(\eta_1, \eta_2) &= \frac{\Gamma(2\ell+2)\Gamma(-i\eta_-)e^{-\pi\eta_1}}{\Gamma(1+\ell-i\eta_1)\Gamma(1+\ell+i\eta_2)} \\
 &= \frac{\Gamma(2\ell+2)\Gamma(-i\eta_-)\Gamma(1+\ell+i\eta_1)\Gamma(1+\ell-i\eta_2)e^{-\pi\eta_1}}{|\Gamma(1+\ell-i\eta_1)\Gamma(1+\ell+i\eta_2)|} \\
 &= \Gamma(-i\eta_-)\Gamma(1+\ell+i\eta_1)\Gamma(1+\ell-i\eta_2)\Xi_\ell. \tag{A18}
 \end{aligned}$$

Here we have

$$\Xi_\ell = \frac{\Gamma(2\ell+2)e^{-\pi\eta_1}}{|\Gamma(1+\ell-i\eta_1)\Gamma(1+\ell+i\eta_2)|} \tag{A19a}$$

$$\Xi_0 = \frac{\text{Sinh}(\pi\eta_1)\text{Sinh}(\pi\eta_2)e^{-\pi\eta_1}}{\pi^2\eta_1\eta_2} \tag{A19b}$$

$$\Xi_1 = \frac{\text{Sinh}(\pi\eta_1)\text{Sinh}(\pi\eta_2)e^{-\pi\eta_1}}{\pi^2\eta_1\eta_2} \frac{6}{(1+\eta_1^2)(1+\eta_2^2)}. \tag{A19c}$$

This also shows that

$$\mathcal{F}(\eta_1, \eta_2) = \frac{4\pi^2\eta_1\eta_2}{(1-e^{-2\pi\eta_1})(1-e^{-2\pi\eta_2})} \equiv \frac{e^{\pi\eta_2}}{\Xi_0}, \tag{A20}$$

which appears in the normalization of the non-relativistic Gaunt factor.

APPENDIX B: LOW-FREQUENCY APPROXIMATION FOR THE GAUNT FACTOR

At low frequencies, the calculation of the Gaunt factor for the non-relativistic limit become highly unstable. To obtain an approximation at low frequencies we take the limits of G_ℓ for $\eta_2 \rightarrow \eta_1$. With $z = -1/x = \eta_-^2/4\eta_1\eta_2$, this yields

$$G_0 \approx 2 \left(\text{Re} [\Lambda_0] \cos \left[\frac{\eta_-}{2} \ln(z) \right] - \text{Im} [\Lambda_0] \sin \left[\frac{\eta_-}{2} \ln(z) \right] \right)$$

$$\Delta G = \left[\eta_1\eta_2 + \frac{1}{2} \left(\frac{\eta_1}{\eta_2} + \frac{\eta_2}{\eta_1} \right) \right] G_0 - \frac{(1+\eta_1^2)(1+\eta_2^2)}{6} G_1$$

$$\approx 4\eta_- \left(\text{Im} [\Lambda_0] \cos \left[\frac{\eta_-}{2} \ln(z) \right] - \text{Re} [\Lambda_0] \sin \left[\frac{\eta_-}{2} \ln(z) \right] \right)$$

$$\text{Re} [\Lambda_0] \approx -\frac{1-e^{-2\pi\eta_1}}{2\pi\eta_1} \text{Re} [H(i\eta_1)]$$

$$\text{Im} [\Lambda_0] \approx -\frac{1-e^{-2\pi\eta_1}}{2\pi\eta_1} \text{Im} [H(i\eta_1)] + \frac{1}{\eta_-}, \tag{B1}$$

where $H(z)$ denotes the harmonic number of z . From this one finds

$$g_{\text{NR}}(\omega, p_1) \approx \frac{\sqrt{3}}{\pi} \mathcal{F}_E(\eta_1, \eta_2) C_0(\eta_1, \eta_2) \Delta C(\eta_1, \eta_2)$$

$$\mathcal{F}_E(\eta_1, \eta_2) = \frac{\eta_2}{\eta_1} \frac{1-e^{-2\pi\eta_1}}{1-e^{-2\pi\eta_2}},$$

$$\Sigma_1 = \text{Re} [H(i\eta_1)], \quad \Sigma_2 = \text{Im} [H(i\eta_1)] - \frac{1}{\Delta\eta}, \tag{B2}$$

$$C_0(\eta_1, \eta_2) = \Sigma_1 \cos \left[\frac{\Delta\eta}{2} \ln(-x) \right] + \Sigma_2 \sin \left[\frac{\Delta\eta}{2} \ln(-x) \right]$$

$$\Delta C(\eta_1, \eta_2) = \eta_- \left(\Sigma_2 \cos \left[\frac{\Delta\eta}{2} \ln(-x) \right] + \Sigma_1 \sin \left[\frac{\Delta\eta}{2} \ln(-x) \right] \right),$$

with $\Delta\eta = \eta_- = \eta_1 - \eta_2$. Since at low frequencies $\Delta\eta \ll 1$, one can set $\cos \left[\frac{\Delta\eta}{2} \ln(-x) \right] \approx 1$ and $\sin \left[\frac{\Delta\eta}{2} \ln(-x) \right] \approx \frac{\Delta\eta}{2} \ln(-x)$. Equation (B2) therefore further simplifies to the expression given in Eq. (4).

To evaluate the real and imaginary parts of the harmonic number we use the explicit series when $0 < \eta_1 < 10$:

$$\text{Re} [H(ia)] = \sum_{m=1}^a \frac{a^2}{m(a^2+m^2)}, \quad \text{Im} [H(ia)] = \sum_{m=1}^a \frac{a}{(a^2+m^2)}, \tag{B3}$$

while for large argument we have

$$\begin{aligned}
 \text{Re} [H(ia)] &\approx \gamma_E + \ln a + \frac{1}{12a} \left(1 + \frac{1}{10a^2} + \frac{1}{21a^4} + \frac{1}{20a^6} + \frac{1}{11a^8} \right) \\
 \text{Im} [H(ia)] &\approx \frac{\pi}{2} - \frac{1}{2a} + 2\pi \left[\coth \left(\frac{\pi}{a} \right) - 1 \right], \tag{B4}
 \end{aligned}$$

where γ_E is the Euler-constant. These approximation are extremely useful at very low frequencies, $\omega/\omega_{\text{max}} \lesssim 10^{-6}$, and large η_1 , i.e., $p_1 \lesssim 10^{-3}$.

APPENDIX C: EH CROSS SECTION

The starting point for our computations is the EH cross section (Elwert & Haug 1969). We shall use all definitions as in Sect. 2 and add the auxiliary variables

$$\mu_i = \frac{\mathbf{p}_i \cdot \mathbf{k}}{p_i \omega}, \quad \kappa_i = 2(\gamma_i - p_i \mu_i) = 2(\gamma_i - \pi_i) \quad (\text{C1a})$$

$$\mu_{12} = \frac{\mathbf{p}_1 \cdot \mathbf{p}_2}{p_1 p_2} = \mu_1 \mu_2 + \cos(\phi_2) \sqrt{1 - \mu_1^2} \sqrt{1 - \mu_2^2} \quad (\text{C1b})$$

$$\pi_i = p_i \mu_i, \quad \pi_{12} = p_1 p_2 \mu_{12}, \quad \eta_\infty = \alpha Z, \quad \eta_\pm = \eta_1 \pm \eta_2 \quad (\text{C1c})$$

$$\chi_i = p_i \sqrt{1 - \mu_i^2}, \quad \chi_{12} = \chi_1 \chi_2 \cos(\phi_2) \quad (\text{C1d})$$

$$\tau_i = 4\gamma_i^2 - q^2, \quad \tau_{12} = 4\gamma_1 \gamma_2 - q^2, \quad \zeta_i = \chi_i^2 - \chi_{12}, \quad (\text{C1e})$$

$$q^2 = |\mathbf{p}_1 - \mathbf{p}_2 - \mathbf{k}|^2 = p_1^2 + p_2^2 + \omega^2 + 2[\omega(\pi_2 - \pi_1) - \pi_{12}] \quad (\text{C1f})$$

$$\xi = \frac{\tilde{\mu} q^2}{\kappa_1 \kappa_2}, \quad \tilde{\mu} = \frac{\mu}{\omega^2} = \left(\frac{p_1 + p_2}{\omega} \right)^2 - 1 \equiv \frac{2(\gamma_1 \gamma_2 + p_1 p_2 - 1)}{\omega^2}, \quad (\text{C1g})$$

$$\rho = \frac{1}{p_1} + \frac{1}{p_2}, \quad \kappa = \frac{\gamma_1}{p_1} + \frac{\gamma_2}{p_2}, \quad (\text{C1h})$$

for further convenience. The Gaunt factor (differential in three angles) can then be written as (Elwert & Haug 1969)

$$\frac{d^3 g_{\text{EH}}}{d\mu_1 d\mu_2 d\phi_2} = \frac{3\sqrt{3}}{8\pi^2} p_1 p_2 \mathcal{F}(\eta_1, \eta_2) \mathcal{M}^2(\omega, p_1, \mu_1, \mu_2, \phi_2) \quad (\text{C2a})$$

$$\mathcal{M}^2 = \frac{e^{-2\pi\eta_1}}{q^4} \left\{ \frac{E_1}{\kappa_1^2} |A_1|^2 + \frac{E_2}{\kappa_2^2} |A_2|^2 - \frac{2E_3}{\kappa_1 \kappa_2} \text{Re}[A_1^* A_2] \right. \\ \left. + \frac{F_3 q^4}{\kappa_1^2 \kappa_2^2} |B|^2 - \frac{2q^2 (F_1 \kappa_2 \text{Re}[A_1^* B] + F_2 \kappa_1 \text{Re}[A_2^* B])}{\kappa_1^2 \kappa_2^2} \right\}. \quad (\text{C2b})$$

Here \mathcal{M}^2 depends on the following functions:

$$V(\eta_1, \eta_2, \xi) = {}_2F_1(i\eta_1, i\eta_2, 1, 1 - \xi) \quad (\text{C2c})$$

$$W(\eta_1, \eta_2, \xi) = {}_2F_1(1 + i\eta_1, 1 + i\eta_2, 2, 1 - \xi) = \frac{1}{\eta_1 \eta_2} \partial_\xi V(\eta_1, \eta_2, \xi) \quad (\text{C2d})$$

$$A_i = V - i\xi \eta_i W, \quad B = i\eta_\infty W \quad (\text{C2e})$$

$$E_1 = (4\gamma_2^2 - q^2) \chi_1^2 + \left[\chi_1^2 - \chi_{12} + 2(1 + \chi_2^2) \right] \frac{\omega}{\kappa_2} \kappa_1 \omega \quad (\text{C2f})$$

$$E_2 = (4\gamma_1^2 - q^2) \chi_2^2 - \left[\chi_2^2 - \chi_{12} - 2(1 + \chi_1^2) \right] \frac{\omega}{\kappa_1} \kappa_2 \omega \quad (\text{C2g})$$

$$E_3 = (4\gamma_1 \gamma_2 - q^2) \chi_{12} + 2(1 + \chi_{12}) \omega^2 \\ + \left[(\chi_1^2 - \chi_{12}) \kappa_2 - (\chi_2^2 - \chi_{12}) \kappa_1 \right] \frac{\omega}{2} \quad (\text{C2h})$$

$$F_1 = \rho(\chi_1^2 - \chi_{12}) + \kappa \left[\pi_1(\pi_{12} + p_2^2) + (2 - \pi_1 \pi_2) \omega \right] \quad (\text{C2i})$$

$$- \left(\kappa p_1 p_2 - 2 \frac{\omega}{p_1} \right) [\pi_1 + \pi_2 - \omega] \quad (\text{C2j})$$

$$F_2 = \rho(\chi_2^2 - \chi_{12}) + \kappa \left[\pi_2(\pi_{12} + p_1^2) - (2 - \pi_1 \pi_2) \omega \right] \quad (\text{C2k})$$

$$- \left(\kappa p_1 p_2 + 2 \frac{\omega}{p_2} \right) [\pi_1 + \pi_2 + \omega] \quad (\text{C2l})$$

$$F_3 = \mu \left[1 - \frac{\pi_1 \pi_2}{p_1 p_2} + \frac{\gamma_1 + \gamma_2}{p_1 p_2} \frac{\gamma_1 + \gamma_2 + \pi_1 + \pi_2}{p_1 p_2} \right] - 2\rho^2. \quad (\text{C2m})$$

We followed the original definitions as closely as possible but already performed a few trivial simplifications. A few symmetries are worth noting. The function E_2 can be obtained from E_1 by switching the roles of $\mathbf{p}_1 \leftrightarrow \mathbf{p}_2$ and negating $\omega \rightarrow -\omega$ or equivalently $\mathbf{k} \rightarrow -\mathbf{k}$. The function E_3 remains invariant under this transformation. Similar statements apply to the F_i 's.

It is difficult to work with the matrix element in the above form, which furthermore suffers from severe numerical cancellation issues. To simplify matters, we collect all coefficients of the main functions that are appearing.

These are $\propto |V|^2$, $\propto \text{Im}[V^* W]$ and $\propto |W|^2$ and after gathering terms we find

$$|A_i|^2 = |V|^2 + 2\eta_i \xi \text{Im}[V^* W] + \eta_i^2 \xi^2 |W|^2 \quad (\text{C3a})$$

$$|B|^2 = \eta_\infty^2 |W|^2 \quad (\text{C3b})$$

$$\text{Re}[A_1^* A_2] = |V|^2 + \eta_+ \xi \text{Im}[V^* W] + \eta_1 \eta_2 \xi^2 |W|^2 \quad (\text{C3c})$$

$$\text{Re}[A_i^* B] = -\eta_\infty \text{Im}[V^* W] - \eta_i \eta_\infty \xi |W|^2. \quad (\text{C3d})$$

We also note that in comparison to EH a factor of $e^{-2\pi\eta_1}$ can be absorbed into the definitions of V and W , since it is canceled directly by a corresponding factor from the hypergeometric function, and thus avoids spurious numerical instabilities for $p_1 \ll 1$. By regrouping terms we then find

$$\mathcal{M}^2 = \frac{e^{-2\pi\eta_1}}{q^4} \left\{ \left(\frac{E_1}{\kappa_1^2} + \frac{E_2}{\kappa_2^2} - \frac{2E_3}{\kappa_1 \kappa_2} \right) |V|^2 + 2\xi \left[\frac{\eta_1 E_1}{\kappa_1^2} + \frac{\eta_2 E_2}{\kappa_2^2} - \frac{E_3 \eta_+}{\kappa_1 \kappa_2} \right. \right. \\ \left. \left. + \left(\frac{F_1}{\kappa_1} + \frac{F_2}{\kappa_2} \right) \frac{\eta_\infty}{\tilde{\mu}} \right] \text{Im}[V^* W] + \xi^2 \left[\frac{\eta_1^2 E_1}{\kappa_1^2} + \frac{\eta_2^2 E_2}{\kappa_2^2} - \frac{2E_3 \eta_1 \eta_2}{\kappa_1 \kappa_2} \right. \right. \\ \left. \left. + \left(\frac{\eta_1 F_1}{\kappa_1} + \frac{\eta_2 F_2}{\kappa_2} \right) \frac{2\eta_\infty}{\tilde{\mu}} + F_3 \frac{\eta_\infty^2}{\tilde{\mu}^2} \right] |W|^2 \right\}, \quad (\text{C4})$$

where we used $q^2/\kappa_1 \kappa_2 = \xi/\tilde{\mu}$. After simplifying the expressions and defining $\mathcal{V} = e^{-\pi\eta_1} V$ and $\mathcal{W} = -\xi e^{-\pi\eta_1} W$ this then yields

$$\mathcal{M}^2 = \frac{1}{q^4} \left\{ J_1 |\mathcal{V}|^2 - 2J_2 \text{Im}[\mathcal{V}^* \mathcal{W}] + J_3 |\mathcal{W}|^2 \right\} \quad (\text{C5a})$$

$$J_1 \equiv J_{\text{BH}} = \tau_1 \frac{\chi_2^2}{\kappa_2^2} + \tau_2 \frac{\chi_1^2}{\kappa_1^2} - \tau_{12} \frac{2\chi_{12}}{\kappa_1 \kappa_2} + (\zeta_1 + \zeta_2) \frac{2\omega^2}{\kappa_1 \kappa_2} \quad (\text{C5b})$$

$$J_2 = \tau_1 \frac{\eta_2 \chi_2^2}{\kappa_2^2} + \tau_2 \frac{\eta_1 \chi_1^2}{\kappa_1^2} - \tau_{12} \frac{\eta_+ \chi_{12}}{\kappa_1 \kappa_2} + \frac{\eta_-}{2} \left(\frac{\zeta_1}{\kappa_1} + \frac{\zeta_2}{\kappa_2} \right) \omega \\ + (\eta_1 \zeta_2 + \eta_2 \zeta_1) \frac{2\omega^2}{\kappa_1 \kappa_2} + \left(\frac{F_1}{\kappa_1} + \frac{F_2}{\kappa_2} \right) \frac{\eta_\infty}{\tilde{\mu}} \quad (\text{C5c})$$

$$J_3 = \tau_1 \frac{\eta_2^2 \chi_2^2}{\kappa_2^2} + \tau_2 \frac{\eta_1^2 \chi_1^2}{\kappa_1^2} - \tau_{12} \frac{2\eta_1 \eta_2 \chi_{12}}{\kappa_1 \kappa_2} + \eta_- \left(\frac{\eta_1 \zeta_1}{\kappa_1} + \frac{\eta_2 \zeta_2}{\kappa_2} \right) \omega \\ + \left[\eta_1^2 \zeta_2 + \eta_2^2 \zeta_1 + \eta_-^2 (1 + \chi_{12}) \right] \frac{2\omega^2}{\kappa_1 \kappa_2} \\ + \left(\frac{\eta_1 F_1}{\kappa_1} + \frac{\eta_2 F_2}{\kappa_2} \right) \frac{2\eta_\infty}{\tilde{\mu}} + F_3 \frac{\eta_\infty^2}{\tilde{\mu}^2}. \quad (\text{C5d})$$

The function J_1 contains all terms relevant to the Bethe-Heitler approximation. Even if written in this way the matrix element already becomes more transparent, further simplifications are possible. Firstly, we have the identity

$$\frac{\eta_-}{2} \omega + \rho \frac{\eta_\infty}{\tilde{\mu}} \equiv 0 \quad \longleftrightarrow \quad \frac{\eta_\infty}{\tilde{\mu}} = -\frac{\eta_- \omega}{2\rho} \quad (\text{C6})$$

This eliminates the ρ -terms from F_1 and F_2 while canceling those directly $\propto \omega$ in J_2 and J_3 :

$$J_2 = \tau_1 \frac{\eta_2 \chi_2^2}{\kappa_2^2} + \tau_2 \frac{\eta_1 \chi_1^2}{\kappa_1^2} - \tau_{12} \frac{\eta_+ \chi_{12}}{\kappa_1 \kappa_2} \\ + (\eta_1 \zeta_2 + \eta_2 \zeta_1) \frac{2\omega^2}{\kappa_1 \kappa_2} + \left(\frac{\tilde{F}_1}{\kappa_1} + \frac{\tilde{F}_2}{\kappa_2} \right) \frac{\eta_\infty}{\tilde{\mu}} \quad (\text{C7a})$$

$$J_3 = \tau_1 \frac{\eta_2^2 \chi_2^2}{\kappa_2^2} + \tau_2 \frac{\eta_1^2 \chi_1^2}{\kappa_1^2} - \tau_{12} \frac{2\eta_1 \eta_2 \chi_{12}}{\kappa_1 \kappa_2} + \frac{\eta_-^2 \omega^2}{2} \\ + \left[\eta_1^2 \zeta_2 + \eta_2^2 \zeta_1 + \eta_-^2 (1 + \chi_{12}) \right] \frac{2\omega^2}{\kappa_1 \kappa_2} \\ + \left(\frac{\eta_1 \tilde{F}_1}{\kappa_1} + \frac{\eta_2 \tilde{F}_2}{\kappa_2} \right) \frac{2\eta_\infty}{\tilde{\mu}} + F_3 \frac{\eta_\infty^2}{\tilde{\mu}^2} \quad (\text{C7b})$$

with $\tilde{F}_i = F_i(\rho = 0)$. The J_1 terms are most relevant in the Bethe-Heitler

regime, and we thus recast J_2 and J_3 as

$$J_2 = \eta_1 J_1 - \eta_- \Delta_1, \quad J_3 = \eta_1^2 J_1 - 2\eta_1 \eta_- \Delta_1 + \eta_-^2 \Delta_2 \quad (\text{C8a})$$

$$\Delta_1 = \frac{\tau_1 \chi_2^2}{\kappa_2^2} - \frac{\tau_{12} \chi_{12}}{\kappa_1 \kappa_2} + \zeta_1 \frac{2\omega^2}{\kappa_1 \kappa_2} + \left(\frac{L_1}{\kappa_1} + \frac{L_2}{\kappa_2} \right) \frac{\omega}{2\rho} \quad (\text{C8b})$$

$$\Delta_2 = \frac{\tau_1 \chi_2^2}{\kappa_2^2} + (1 + \chi_1^2) \frac{2\omega^2}{\kappa_1 \kappa_2} + \frac{L_2}{\kappa_2} \frac{\omega}{\rho} + F_3 \frac{\omega^2}{4\rho^2} \quad (\text{C8c})$$

$$L_1 = \kappa \left[\pi_1 (\pi_{12} + p_2^2) - (\pi_1 + \pi_2 - \omega) p_1 p_2 + (2 - \pi_1 \pi_2) \omega \right] + 2 \frac{\omega}{p_1} (\pi_1 + \pi_2 - \omega) \quad (\text{C8d})$$

$$L_2 = \kappa \left[\pi_2 (\pi_{12} + p_1^2) - (\pi_1 + \pi_2 + \omega) p_1 p_2 - (2 - \pi_1 \pi_2) \omega \right] - 2 \frac{\omega}{p_2} (\pi_1 + \pi_2 + \omega) \quad (\text{C8e})$$

Inserting these expression back into Eq. (C5) and collecting terms we find

$$\mathcal{M}^2 = \frac{1}{q^4} \left\{ J_1 |\mathcal{A}|^2 - 2\eta_- \Delta_1 |C|^2 + \eta_-^2 \Delta_2 |\mathcal{W}|^2 \right\} \quad (\text{C9a})$$

$$|\mathcal{A}|^2 = |\mathcal{V}|^2 - 2\eta_1 \text{Im}[\mathcal{V}^* \mathcal{W}] + \eta_1^2 |\mathcal{W}|^2 \quad (\text{C9b})$$

$$|C|^2 = \eta_1 |\mathcal{W}|^2 - \text{Im}[\mathcal{V}^* \mathcal{W}] \quad (\text{C9c})$$

Expressed in this way indeed simplifies the evaluation of the cross section significantly and also allows one to more easily read off limiting cases.

To explicitly evaluate the functions $|\mathcal{A}|^2$ and $|\mathcal{W}|^2$ we used precomputed tables obtained with *Mathematica* to improve the precision as well as the Gauss series for the hypergeometric function. As shown below, this also determines $|C|^2$ at no additional cost [see Eq. (C14)]. At low frequencies ($\omega \lesssim 10^{-6}$), one can furthermore apply

$$|\mathcal{A}|^2 \approx \left(\frac{1 - e^{-2\pi\eta_1}}{2\pi\eta_1} \right)^2 \left[1 - \frac{2\eta_1^2}{\xi} (1 + \phi) \right] \\ |\mathcal{W}|^2 \approx \left(\frac{1 - e^{-2\pi\eta_1}}{2\pi\eta_1} \right)^2 \left[\phi^2 \left(1 + \frac{2}{\xi} \right) + \frac{2\eta_1^2}{\xi} \phi(2 + \phi) \right] \\ \phi = \ln \xi - 2 \text{Re}[H(i\eta_1)] \quad (\text{C10})$$

to ease the computations. However, the methods relying on G_0 and G'_0 (next section) was found to be more efficient.

C1 Relating \mathcal{V} and \mathcal{W} to G_0

While in principle we can already compute the EH cross section using the expression from the preceding section, one additional obstacle can be overcome by directly relating the function \mathcal{V} and \mathcal{W} to G_0 and G'_0 . One of the important benefits is that G_0 and G'_0 are a real valued function and thus greatly simplify matters. Progress can be made by starting from the differential equation for V , which with $z = 1 - \xi$ reads

$$0 = z(1-z)V'' + [1 - (1+i\eta_+)z]V' + \eta_1 \eta_2 V \\ = -\eta_1 \eta_2 \{z(1-z)W' + [1 - (1+i\eta_+)z]W - V\} \\ \Rightarrow V = [(1-z) - i\eta_+ z]W + z(1-z)W'. \quad (\text{C11})$$

Here primes denote derivatives with respect to z . By comparing W with G_0 we find

$$W = \frac{e^{\pi\eta_1} (1-z)^{-\frac{i\eta_+}{2}}}{-z} G_0(z) \quad \leftrightarrow \quad \mathcal{W} = \frac{(1-z)^{1-\frac{i\eta_+}{2}}}{z} G_0(z), \quad (\text{C12})$$

which directly implies

$$|\mathcal{W}|^2 = \frac{\xi^2 G_0^2(1-\xi)}{(1-\xi)^2} \equiv \xi^2 e^{-2\pi\eta_1} {}_2F_1(1+i\eta_1, 1+i\eta_2, 2, 1-\xi)^2 \quad (\text{C13})$$

We then also have

$$W' = \frac{e^{\pi\eta_1} (1-z)^{-\frac{i\eta_+}{2}}}{-z^2(1-z)} \left[z(1-z)G'_0(z) - (1-z)G_0(z) + i\frac{\eta_+}{2} zG_0(z) \right] \\ V = e^{\pi\eta_1} (1-z)^{-\frac{i\eta_+}{2}} \left\{ i\frac{\eta_+}{2} G_0(z) - (1-z)G'_0(z) \right\},$$

which related both W' and V to G_0 and G'_0 only.

Since $|\mathcal{V}|^2 = e^{-2\pi\eta_1} |\mathcal{W}|^2$, this then yields

$$|\mathcal{V}|^2 = \frac{\eta_+^2}{4} G_0^2(z) + (1-z)^2 [G'_0(z)]^2 \\ \text{Im}[\mathcal{V}^* \mathcal{W}] = -\frac{\eta_+}{2} \frac{(1-z)}{z} G_0^2(z) = -\frac{\eta_+}{2} \frac{z}{1-z} |\mathcal{W}|^2$$

Putting everything together we finally obtain

$$|\mathcal{A}|^2 = \frac{(\eta_+ + \eta_- \xi)^2}{4\xi^2} |\mathcal{W}|^2 + \xi^2 [G'_0(1-\xi)]^2 \quad (\text{C14a})$$

$$|C|^2 = \frac{(\eta_+ + \eta_- \xi)}{2\xi} |\mathcal{W}|^2 \quad (\text{C14b})$$

$$|\mathcal{W}|^2 = \frac{\xi^2 G_0^2(1-\xi)}{(1-\xi)^2}, \quad (\text{C14c})$$

which eliminates the need to compute $|C|^2$ explicitly. Collecting terms then results in

$$\mathcal{M}^2 = \frac{1}{q^4} \left\{ \left[J_1 - 2\delta D_1 + \delta^2 D_2 \right] \frac{\eta_+^2 G_0^2(1-\xi)}{4(1-\xi)^2} + J_1 [\xi G'_0(1-\xi)]^2 \right\} \\ \delta = \frac{\eta_-}{\eta_+} \xi, \quad D_1 = 2\Delta_1 - J_1, \quad D_2 = J_1 - 4\Delta_1 + 4\Delta_2. \quad (\text{C15})$$

This definition groups terms of similar order of magnitude in η_\pm and ξ . Inserting the definitions of Δ_i and simplifying the expression then gives Eq. (11) for the EH matrix element.

REFERENCES

- Bethe H., Heitler W., 1934, Proceedings of the Royal Society of London Series A, 146, 83
Blumenthal G. R., Gould R. J., 1970, Reviews of Modern Physics, 42, 237
Brussaard P. J., van de Hulst H. C., 1962, Reviews of Modern Physics, 34, 507
Cavaliere A., Fusco-Femiano R., 1976, A&A, 500, 95
Chluba J., 2014, MNRAS, 440, 2544
Chluba J., Sunyaev R. A., 2012, MNRAS, 419, 1294
Chluba J., Vasil G. M., Dursi L. J., 2010, MNRAS, 407, 599
Elwert G., 1939, Annalen der Physik, 426, 178
Elwert G., Haug E., 1969, Physical Review, 183, 90
Gaunt J. A., 1930, Zeitschrift für Physik, 59, 508
Gursky H., Solinger A., Kellogg E. M., Murray S., Tananbaum H., Giacconi R., Cavaliere A., 1972, ApJL, 173, L99
Haug E., 1975, Physics Letters A, 54, 339
Haug E., 1985, Phys.Rev.D, 31, 2120
Haug E., 2008, Radiation Physics and Chemistry, 77, 207
Haug E., 2010, European Physical Journal D, 58, 297
Hu W., Silk J., 1993, Phys.Rev.D, 48, 485
Hummer D. G., 1988, ApJ, 327, 477
Itoh N., et. al., 2000, ApJS, 128, 125
Itoh N., Kawana Y., Nozawa S., 2002, Nuovo Cimento B Serie, 117, 359
Itoh N., Nakagawa M., Kohyama Y., 1985, ApJ, 294, 17
Jauch J. M., Rohrlich F., 1976, The theory of photons and electrons. Springer
Johnson L. C., 1972, ApJ, 174, 227
Karzas W. J., Latter R., 1961, ApJS, 6, 167
Kellogg E., Baldwin J. R., Koch D., 1975, ApJ, 199, 299
Kramers H. A., 1923, The London, Edinburgh, and Dublin Philosophical Magazine and Journal of Science, 46, 836
Lucca M., Schöneberg N., Hooper D. C., Lesgourgues J., Chluba J., 2019, arXiv e-prints, arXiv:1910.04619
McKinney J. C., Chluba J., Wielgus M., Narayan R., Sadowski A., 2017, MNRAS, 467, 2241
Menzel D. H., Pekeris C. L., 1935, MNRAS, 96, 77
Narayan R., Yi I., 1995, ApJ, 452, 710
Nozawa S., Itoh N., Kohyama Y., 1998, ApJ, 507, 530
Planck Collaboration et al., 2016, A&A, 594, A9
Poškus A., 2018, Computer Physics Communications, 232, 237
Poškus A., 2019, Atomic Data and Nuclear Data Tables, 129, 101277

- Roche G., Ducos C., Proriol J., 1972, *Phys.Rev.A*, 5, 2403
- Rybicki G. B., Lightman A. P., 1979, *Radiative processes in astrophysics*.
New York, Wiley-Interscience, 1979. 393 p.
- Sarazin C. L., 1986, *Reviews of Modern Physics*, 58, 1
- Shakura N. I., Sunyaev R. A., 1973, *A&A*, 24, 337
- Sommerfeld A., 1931, *Annalen der Physik*, 403, 257
- Sommerfeld A., Maue A. W., 1935, *Annalen der Physik*, 415, 589
- Sunyaev R. A., Zeldovich Y. B., 1970a, *ApSS*, 7, 20
- Sunyaev R. A., Zeldovich Y. B., 1970b, *Comments on Astrophysics and
Space Physics*, 2, 66
- Tseng H. K., Pratt R. H., 1971, *Phys.Rev.A*, 3, 100
- van Hoof P. A. M., Ferland G. J., Williams R. J. R., Volk K., Chatzikos
M., Lykins M., Porter R. L., 2015, *MNRAS*, 449, 2112
- van Hoof P. A. M., Williams R. J. R., Volk K., Chatzikos M., Ferland G. J.,
Lykins M., Porter R. L., Wang Y., 2014, *MNRAS*, 444, 420